UNIVERSITY OF ZAGREB
FACULTY OF MECHANICAL ENGINEERING AND NAVAL ARCHITECTURE

MASTER'S THESIS

Antonio Filipović

Zagreb, 2014.

UNIVERSITY OF ZAGREB
FACULTY OF MECHANICAL ENGINEERING AND NAVAL ARCHITECTURE

MASTER´S THESIS

Supervisors:

Pentti Kujala, Professor (Aalto University)
JoškoParunov, Professor (University of Zagreb)

Student:

Antonio Filipović

Zagreb, 2014.

I declare that I have done this work independently using the knowledge acquired during studies and cited references.

This thesis was written at the Department of Applied Mechanics of Aalto University in academic year 2013/14.

I would like to express my gratitude to Professor Pentti Kujala for being my supervisor and giving me advices. I would also like to thank Mikko Suominen for valuable comments and guidance during the thesis writing process.

Acknowledgments to Professor Joško Parunov for being my supervisor from University of Zagreb side.

I am also grateful to my parents, brother and two sisters for supporting me during my studies, especially during my studies in Finland. Special thanks to my girlfriend, Afrodita, for the support and patience during this work.

Antonio Filipović

SVEUČILIŠTE U ZAGREBU
FAKULTET STROJARSTVA I BRODOGRADNJE
Središnje povjerenstvo za završne i diplomske ispite
Povjerenstvo za završne i diplomske ispite studija brodogradnje

Sveučilište u Zagrebu Fakultet strojarstva i brodogradnje	
Datum	Prilog
Klasa:	
Ur. broj:	

DIPLOMSKI ZADATAK

Student: **Antonio Filipović** Mat. br.: 0135201398

Naslov rada na hrvatskom jeziku: **ODREĐIVANJE OPTEREĆENJA BRODSKE KONSTRUKCIJE USLIJED SABIJAJUĆEG LEDA**

Naslov rada na engleskom jeziku: **EVALUATION OF ICE INDUCED LOADS ON SHIPS IN COMPRESSIVE ICE**

Opis zadatka:

Područja prekrivena ledom od velikog su interesa zadnjih desetljeća zbog povećane eksploatacije prirodnih resursa kao i zbog novih transportnih ruta. Trgovački brodovi s dugim paralelnim srednjakom nisu pogodni za zimske uvjete. Sabijajući led može izazvati pritisak na boku broda i brod može zapeti u ledu. Sabijajući led je jedna od najvećih opasnosti za pomorski promet u zimskim uvjetima, no ipak malo se zna o efektima i silama vezanim za taj proces.

U uvodnom dijelu rada je potrebno dati opis sabijajućeg leda kao oceanološke pojave te opterećenja brodske konstrukcije uslijed sabijajućeg leda. Također treba dati pregled odgovarajuće literature i postojećih propisa te mjerenja opterećenja od sabijajućeg leda u naravi.

U proračunskom dijelu rada će se analizirati dostupni podatci modelskih ispitivanja sabijajućeg leda. Podatke treba obraditi na način da se dobije linijsko opterećenje po jedinici duljine koje je pogodno za primjenu u projektiranju brodske konstrukcije. Dobivene rezultate zatim usporediti s mjerenjima u naravi i međunarodnom regulativom.

Na kraju rada je potrebno diskutirati rezultate i izvući odgovarajuće zaključke.

Zadatak zadan:	Rok predaje rada:	Predviđeni datumi obrane:
13. ožujka 2014.	15. svibnja 2014.	21., 22. i 23. svibnja 2014.

Zadatak zadao:
Prof. dr. sc. Joško Parunov

Predsjednik Povjerenstva:
Prof. dr. sc. Nastia Degiuli

Aalto University
School of Engineering

Aalto University,
P.O. BOX 11000, 00076 AALTO
www.aalto.fi
Abstract of master's thesis

Author Antonio Filipović

Title of thesis Evaluation of ice induced loads on ships in compressive ice

Department Department of Applied Mechanics

Professorship Naval Architecture **Code of professorship** Kul-24

Thesis supervisor Professor Pentti Kujala

Thesis advisor Mikko Suominen M.Sc.

Date 13.03.2014. **Number of pages** 54 **Language** English

Abstract

Ice covered sea areas was given more attention during the last decade due to the increased natural resource exploitation and new transport routes. Merchant ships with a long parallel midbody section aren't suitable for winter conditions. Compressive ice can cause pressure to the side of the ship and ship can get stuck in ice. Compressive ice is one of the greatest hazards for maritime traffic in winter conditions, yet little is known about the effects and forces involved.

Within project called SAFEWIN ice model tests were conducted in the ice basin of Aalto University in compressive ice field. Tests included six test series with varying ice thickness and compression levels. The model adopted in the tests was a bulk carrier with a bulbous bow and a long parallel midship section.

In this thesis the loads on the ship model in compressive ice has been studied. Measurement data are gathered from the load panels at the midship, bow shoulder and load sensors on the pusher plates for level ice tests and closing channel tests. Further, natural sea ice is highly heterogeneous and causes high scattering in any measured values. This study seeks to find the maximum line loads caused by compressive ice field and compare those with ones calculated by ISO code to verify ISO code reliability. As a limitation, loads due to ice ridges are not investigated within this thesis.

An analyzed results show that ice thickness has a major influence on the loads. Compression level has influence on loads, too, but significantly less than thickness. Further, line load curves for different ice thicknesses are presented and compared with ISO code. The calculated values represented the results of the model tests fairly well. Moreover, measurements at midship load panel show that weak compression was occurred in 3 out of 6 compressive level ice tests (loads were significantly smaller than in other tests). Comparing compressive level ice and closing channel measurements, loads at the bow shoulder and midship have been found to be higher in closing channel tests.

Keywords compressive ice, ice loads, ice model testing, ship-ice interaction, line load curve, full-scale load

CONTENTS

LIST OF FGURES

LIST OF TABLES

LIST OF SIMBOLS

a	-	unknown parameter
a_{FS}	m/s^2	acceleration in full-scale
a_m	m/s^2	acceleration in model-scale
A_N	m^2	nominal contact area
b	m	width
B	m	breadth
C	-	constant
C_D	-	drag coefficient
C_P	-	coefficient
D	m	ship depth
D_P	MPa	coefficient
E	GPa	Elastic module
E_{FS}	MPa	Elastic module in full-scale
E_m	MPa	Elastic module in model -scale
F	N	force
F'_1	N	force No. 1 measured at the midship load panel
F'_2	N	force No. 2 measured at the midship load panel
F'_3	N	force No. 3 measured at the midship load panel
F_1	N	force measured at the 1st sensor
F_2	N	force measured at the 2nd sensor
F_3	N	force measured at the 3rd sensor
F_4	N	force measured at the 4th sensor
F_5	N	force measured at the 5th sensor
F_6	N	force measured at the 6th sensor
F_7	N	force measured at the 7th sensor
F_8	N	force measured at the 8th sensor
F_{FS}	N	force in full-scale
F_m	N	force in model-scale
F_z	N	force measured on load panel at the bow shoulder in Z direction
h_{cl}	m	consolidate level thickness
h_{FS}	m	ice thickness in full-scale
h_i	m	level ice thickness
h_k	m	thickness of the ridge keel
h_m	m	ice thickness in model-scale
h_s	m	thickness of the ridge sail
h_T	m	characteristic ice thickness
L	m	length

$l_{bowshoulder}$	m	length of the load panel at the bow shoulder
l_c	m	contact length
L_{FS}	m	length in full-scale
L_m	m	length in model-scale
$l_{midship}$	m	length of the load panel at the midship
L_{OA}	m	length overall
L_{PP}	m	length between perpendiculars
p_G	MPa	ice pressure
q	N/m	line load
Q	N/m	line load
Q_{12}	N/m	line load acting on pusher plate 1
Q_{14}	N/m	line load acting on pusher plates 1 and 2
Q_{16}	N/m	line load acting on pusher plates 1, 2 and 3
Q_{18}	N/m	line load acting on all pusher plates
Q_{34}	N/m	line load acting on pusher plate 2
Q_{36}	N/m	line load acting on pusher plates 2 and 3
Q_{38}	N/m	line load acting on pusher plates 2, 3 and 4
Q_{56}	N/m	line load acting on pusher plate 3
Q_{58}	N/m	line load acting on pusher plates 3 and 4
Q_{78}	N/m	line load acting on pusher plate 4
$Q_{bowsholder}$	N/m	line load acting on bow shoulder load panel
q_c	kN/m	limit stress when ridge starts to form
$Q_{midship}$	N/m	line load acting on midship load panel
Q_{PP1}	N/m	the highest line load acting on one pusher plate
Q_{PP2}	N/m	the highest line load acting on two adjacent pusher plates
Q_{PP3}	N/m	the highest line load acting on three pusher plates in sequence
Q_{PP4}	N/m	the highest line load acting on four pusher plates
R	-	ration between consolidate layer thickness and level ice thickness
s	m	the smallest load width obtained by scaling the typical full scale values of frame spacing to model scale
T	m	drought
t_{FS}	s	time in full-scale
t_m	s	time in model-scale
v	m/s	speed
v_{FS}	m/s	speed in full-scale
v_m	m/s	speed in model-scale
w	m	width
λ	-	scaling factor
μ_{FS}	-	coefficient of friction in full-scale
μ_m	-	coefficient of friction in model-scale
ν	-	Poisson’s ratio

ρ	Kg/m^3	density
ρ_{FS}	kg/m3	density in full-scale
ρ_i	Kg/m^3	ice density
ρ_m	kg/m3	density in model -scale
σ_b	kPa	bending strength of ice
σ_c	MPa	compressive strength of ice
σ_f	kPa	flexural strength of ice
σ_{FS}	kPa	stress in full-scale
σ_m	kPa	stress in model-scale
τ	Pa	shear stress

ABBREVATION

AFRAMAX	Size of tanker, deadweight under 120000 tons and breadth more than 32.31 m
ALIE	abnormal-level ice event
ELIE	extreme-level ice event
EU	European Union
FMI	Finnish Meteorological Institute
IMO	International Maritime Organization
ISO	International Organization for Standardization
SAFEWIN	an EU project on Safety of Winter Navigation in Dynamic Ice
SMHI	Swedish Meteorological and Hydrological Institute
US	United States
USSR	The Union of Soviet Socialist Republics

SAŽETAK

Područja prekrivena ledom od velikog su interesa zadnjih desetljeća zbog povećane eksploatacije prirodnih resursa kao i zbog novih transportnih ruta. Trgovački brodovi s dugim paralelnim srednjakom nisu pogodni za zimske uvjete. Sabijajući led može izazvati pritisak na boku broda i brod može zapeti u ledu. Sabijajući led je jedna od najvećih opasnosti za pomorski promet u zimskim uvjetima, no ipak malo se znao o efektima i silama vezanim za taj proces.

U sklopu projekta nazvanog „SAFEWIN“, obavljena su modelska ispitivanja u bazenu s ledom Aalto Sveučilišta u polju sabijenog leda. Ispitivanja uključuju šest ispitnih serija s različitim debljinama leda i stupnjem sabijanja. Model korišten u ispitivanjima je brod za rasuti teret s pramčanim bulbom i dugim paralelnim srednjakom.

U ovom radu su proučavana opterećenja na model u sabijajućem ledu. Upotrijebljeni mjerni podaci su prikupljeni s mjernih panela na paralelnom srednjaku, pramčanom ramenu i senzorima opterećenja na potisnim pločama za ispitivanja nivo leda (eng. level ice tests) i ispitivanja kanala koji se zatvara (eng. closing channel tests). Prirodni morski led je prilično heterogen i uzrokuje veliko rasipanje izmjerenih vrijednosti. Ovim radom se pokušavaju pronaći maksimalne krivulje opterećenja uzrokovane sabijajućim poljem leda i usporediti ih s onima dobivenima prema ISO propisima da bi se potvrdila pouzdanost tih propisa. Kao ograničenje, opterećenja uslijed ledenih grebena nisu promatrana u ovom radu.

Analizirani rezultati pokazuju da debljina leda ima najveći utjecaj na opterećenja. Stupanj sabijanja također ima utjecaj, ali značajno manje nego debljina leda. Nadalje, prikazane su linije opterećenja za različite debljine leda i uspoređene su s ISO propisima. Izračunate vrijednosti jako dobro aproksimiraju rezultate modelskih ispitivanja. Povrh toga, mjerenja na opterećenim panelima na paralelnom srednjaku pokazuju da se slabo sabijanje dogodilo u 3 od 6 ispitivanja (opterećenja su bila značajno manja nego u drugim ispitivanjima). Uspoređujući mjerenja sabijajućeg nivo leda i zatvarajućeg kanala, opterećenja na pramčanom ramenu i paralelnom srednjaku su bila viša u ispitivanima zatvrajućeg kanala.

Ključne riječi: sabijajući led, opterećenje od leda, modelska ispitivanja s ledom, međudjelovanje brod-led, krivulja linijskog opterećenja, opterećenja u punom mjerilo

1. INTRODUCTION

1.1. Background of the study

Efficient and safe winter navigation has been a hot topic for many decades. Today this topic is more discussed than ever. Transport and trade in the Arctic and Baltic are increasing due to the importance of the Russian oil and gas industry (Russia is the second largest oil exporter in the world (see http://www.eia.gov)), as well because of oil reserves in the Arctic region. Export and import trough the sea are of great importance for the Baltic region. This requires ships that can safely operate in ice wasted areas independent or with assistance of icebreakers. Winter shipping has been assisted by icebreakers, and even then transportation systems had suffered from delays. This is the reason why in the last decade interest for ice class vessels is increasing, in oil tanker fleet particularly. An AFRAMAX tanker as a type was frequently required because of limited draught of vessel in transit through strait Skagerak which connects the North Sea with the Baltic Sea. This depth is fulfilled with draught of AFRAMAX size vessel. This rapid rise in transport also caused an increase of the risk of accidents such as: ice induced damage, collision, grounding etc. Furthermore, ice loads on the ship hull in converging ice fields represent one of the most under-researched areas in ship-ice interaction.

As the compressive situation is not widely studied, the amount of data available is limited. Therefore, the Baltic countries, as well as the European Union (EU) and the International Maritime Organization (IMO) are making great efforts to anticipate possible risks of accidents and the consequences, both, economical and environmental, that may occur. Example of this effort is SAFEWIN project, lunched by EU. The project aim is to develop an efficient forecasting system for ice compression and ice dynamics. This should lead to safer winter navigation. The system is intended for AFRAMAX size or larger oil tankers operating in the Baltic, Okhotsk Sea and in the western Russian Arctic. These tankers are not very suitable for icebreaking and can therefore get stuck easier in compressive ice (see http://www.safewin.org).

1.2. State of the art

Even though the behavior and properties of the sea ice have received much attention over the last decades, the dynamics of sea ice is clearly understudied. Numerical methods are of great help for engineers, but they are based on statistic data, in situ measurements and model tests. The first ice model tests in compressive ice field were conducted in a joint research project between Helsinki University of Technology/ Laboratory of Naval Architecture and Marine Engineering, and Academy of Sciences in USSR/ Institute of Problems in Mechanics, called "A Ship in Compressive Ice" [1]. The project carried out in the early 1990's produced valuable data in the form of model test in ice, full scale observations and theories developed throughout the project. The research conducted in the joint project was summarized by Riska et al.[2]. The summary presented an early method to estimate the additional resistance due to compression. In addition, an initial method on predicting ice loads at midship was presented [2].

Leppäranta[3] describes the growth of ice, drift of ice, pressures inside ice cover and forces needed to from ridges. However, the book is focused on geophysics and ridging forces of the ice cover, thus not making the forces applicable for ship-ice interaction calculations without modification. From the marine traffic point of view, compressive ice fields have been addressed in FMA research report no. 59 [4]. This publication presents a description of the compression in general, observations done onboard ice going vessels and the derivation of calculation methods for an operative compression forecast model. A good overview is given of the compressive ice field evolution.

Drift of sea ice fields can be divided into static and dynamic. Static compression is an expression of thermal expansion inside the ice due to the ambient temperature variation. The term dynamic ice in an ice cover refers to a situation where wind and/or current exert drag force on ice cover and the ice starts to drift. There are two cases when the ice drift occurs, the ice field can be divergent or convergent. In a case of divergent ice field, the wind causes the ice field breaks apart creating the leads of open water while overall ice coverage decreases. When wind or current drag acts on open pack ice, the ice floes start to move. If the ice motion is restricted by an obstacle like a shoreline or landfast ice, the ice cover starts to compact. First all the open water areas close. This is followed by rafting of ice at the contact points between ice floes. The rafting is followed by ridging [4]. In that case, the ice field is said to be convergent or compressive. In theory the ridging force is the maximum compressive force which could be present in the ice field. When the forces required to form ridges exceed the driving force, the ice cover is immobile, but the compressive stresses in the ice field remain. An example of a dynamic convergent process in pack ice field is presented in Figure 1. Further, when a ship navigates in the compressive ice field, larger resistance is encountered and the ship might get stuck, as large compression forces are applied on the ship's sides. The converging ice field is not favorable for ships with low propulsion power and/or long parallel midship section, moreover such ice fields can contain enough force for even ice-breakers to get stopped.

Also, it should be noted that during free drift mode, the pack ice field does not experience any compressive forces.

The stresses in the converging ice field have been proposed to have a uniform distribution in a single floe due to the randomness of the contact between the floes. Force of one flow can affect the other only through the contact point, forming a so called stress tree [5]. A schematic presentation of the stress tree is presented in Figure 2. The black circles highlight the contact areas between ice floes through which the forces are transmitted. These force lines, which create the force tree, are generated when the free floating ice floes collide at distinct points and continue compacting due to external forces. The stress in the ice floes is induced from contact areas. It can be assumed that the stress area close to the contact is small/narrow, and therefore the stresses are very local and large. In the middle of the ice floe the stress is divided in to a larger area making the average stress lower [6].

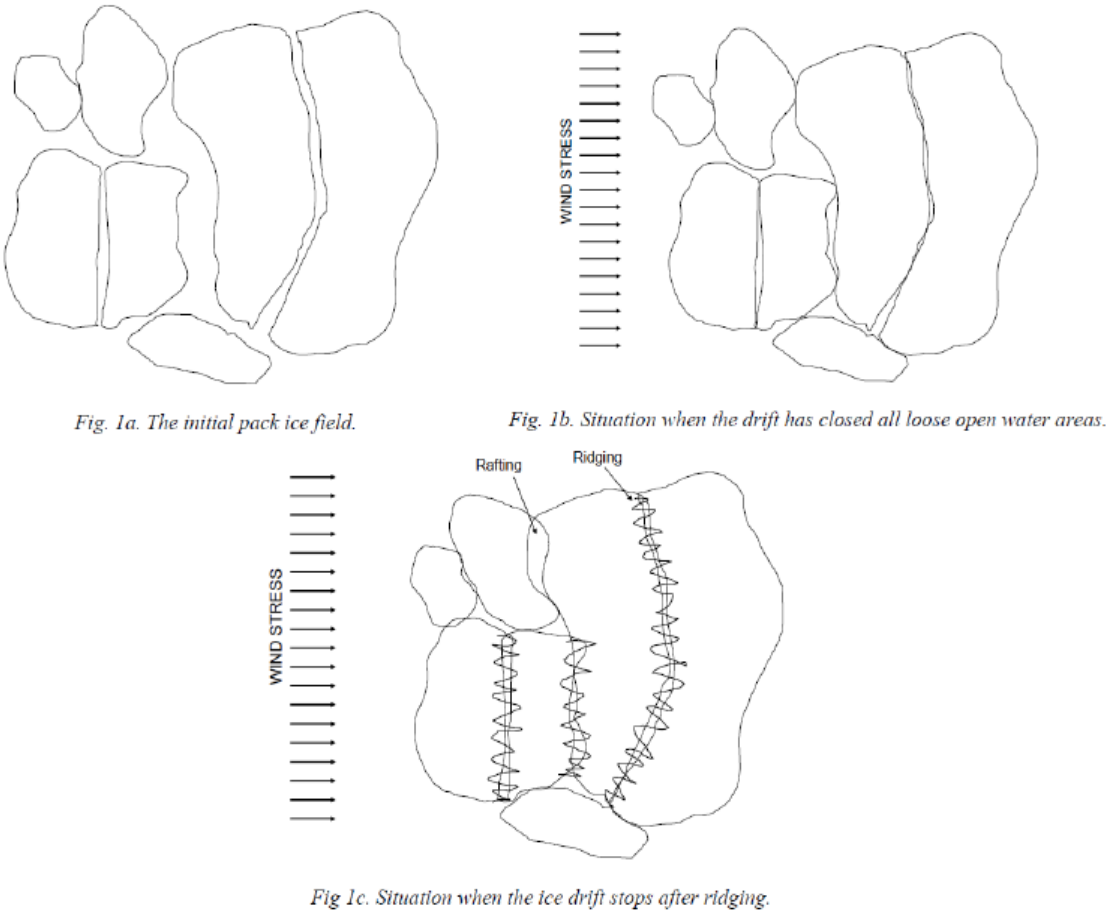

Fig. 1a. The initial pack ice field.

Fig. 1b. Situation when the drift has closed all loose open water areas.

Fig 1c. Situation when the ice drift stops after ridging.

Figure 1 *Convergent ice field* **[4]**.

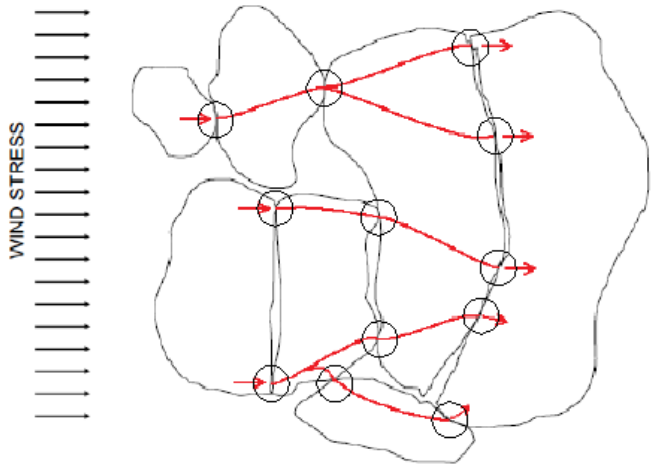

Figure 2 *Schematic stress tree in converging pack-ice field* **[5]**.

This kind of uniform stress distribution can make a converging pack ice field extremely difficult to navigate. According to this theory, there might be no stress in the ice floe between the branches, while all of the wind and current stress is transferred through the stress branches (marked as red lines in Figure 2). Therefore, the crew of a vessel, sailing in this kind of converging ice, might not even notice any movement or ridging in the area, until they get to

the stress branch. In this case, the compressive effects (speed reduction, stopping or damage to the hull) can be extremely local and difficult to predict [6].

Kujala and Arughadhoss[7] studied the ice loading on the model hull equipped with tactile sensor sheets. A series of tests took place over four days in the Aalto ice tank and involved two different ship models. The crushing pressure on a ship's hull was analyzed statistically. The study with the pressure foils showed that the line load decreases at the bow and midship as a function of line load width. The peak pressures caused by ice were calculated from four sensor sheets located at different positions on the hull. Also, based on measurements at the bow, pressure-area curve is presented.

During the SAFEWIN project ice model tests were conducted in the ice basin of Aalto University with a tanker model in compressive ice fields [8]. These tests were conducted in level ice, open channel, compressive level ice and closing channel with different ice thicknesses and ice drift speeds. Model tests were performed with a similar procedure to those conducted during the "A Ship in Compressive Ice" project [2]. In the SAFEWIN project tests the model towing speed was kept as constant. The ice load measurements showed that ice loads on hull mainly occur at bow and bow shoulder area. The measurement results indicate that the added resistance due to dynamic compression results from added line loads at midship area. The resistance was significantly higher in dynamic compression than in static compression or in level ice. Furthermore, study of the closed channel data showed that the ice thickness has an effect on the resistance due to compression as the added resistance increases as a function of ice thickness. In addition, the study with pressure foils showed that the resistance is increasing as a function of contact area.

Also, Suominen and Kujala[9] analyzed results from same tests with focus on the ice load measurements. Authors suggest that the load width needs to be wide enough (on average) that the loading process can be a fully developed loading case and the possibility of maximum local ice load to occur is high. The fully developed loading case refers here to the cases where the ice is broken through the failure mode resulting in the highest possible loads. At midship this would be through crushing and at the bow shoulder through bending. Furthermore, the maximum line load is decreasing as a function of the contact width at the bow shoulder and midship.

Another reference on the SAFEWIN project ice model tests is a M.Sc. thesis by Reino Külaots[10]. In named thesis comparison of model testing results with different calculation methods was done. Additional model tests were performed as one part of this thesis. Results demonstrate that additional resistance tends to decrease at higher vessel speeds, while level ice resistance increases. In moderate ice going speeds, converging ice field can more than double the total resistance of the vessel.

In general, much is still unknown about the behavior of compressive ice and the effect it has on the shipping.

1.3. Aim of the study

The main goal of this thesis is to study the effect of the ice thickness and the level of compression (ice speed) to the ice loads on the model hull. Ice model tests were conducted in Aalto University's ice basin during December 2011 and January 2012. Measurement data is gathered together from the load panels at the midship, bow shoulder and load sensors on the pusher plates. An analysis of the different load conditions, the ice thickness and the compression level, in these model testing is conducted. Furthermore, methods for estimating ice loads from ISO 19906; Global ice pressure from sea ice and Global ice pressure from ship ramming test are presented. The methods are validated using ice model tests, which were conducted within the SAFEWIN project.

2. ICE CONDITION

2.1. Ice conditions in the Baltic Sea

Ice conditions in the Baltic Sea show a very large variation in different winters. Due to the location in the northern latitudes, sea ice can be found in the Baltic Sea areas in a normal winter. The ice conditions in the northern parts of the Baltic Sea, in the Gulf of Finland as well as in the Bay of Bothnia are mostly affected by two factors: the cumulative sum of freezing days and the direction of prevailing winds. The count of freezing days (i.e., the cumulative average temperature of the winter) controls the ice growth and the amount of ice. The prevailing winds control the drifting and ridging of the ice field. The annual variation of the maximum extent of the ice covered area in the Baltic Sea has been great. Most often the ice cover has extended to cover about 20 – 40 % of the Baltic Sea, see Figure 3[11].

Ice formation in the Baltic Sea starts in the northernmost parts of the Bothnian Bay in late October or early November [12]. The ice break-up starts in the southern parts in early March and the northern Bothnian Bay is usually opened again in May. The Gulf of Finland starts to freeze in the beginning of December on an average winter. The average length of the ice season in the Gulf of Finland is 120 days outside St. Petersburg and 30 days at the entrance of the gulf. The maximum level ice thickness is greatest at the eastern pats on the gulf and is about 50 cm on an average winter. In a hard winter the maximum thickness of level ice can be up to 70 cm. The thickness of the ice cover is strongly variable. These variations are caused by thermal and mechanical factors. Moreover, only first year ice exists in the Baltic Sea. Fast ice exists in the Gulf of Finland only at the shores and the whole open sea area is drift ice zone [13].

On a hard winter there exists a great amount of ice and the ice cover is extending to a large area, see Figure 4. Also, the majority of harbors and their surrounding areas in the northern Baltic Sea are covered with ice. On milder winters not necessarily all harbors become icebound, and especially the central areas in the sea basins (e.g. in the Bothnian Sea, the Gulf of Finland and the Baltic Proper) may stay open.

In addition, the salinity of the Baltic Sea is lower than the Oceans (35 ‰), close to Finland, the salinity of surface water is 3-6 ‰ and at bottom 1.4 ‰ higher. The sea water with normal salinity will freeze at -4°C and the Baltic Sea at about -0.3°C.

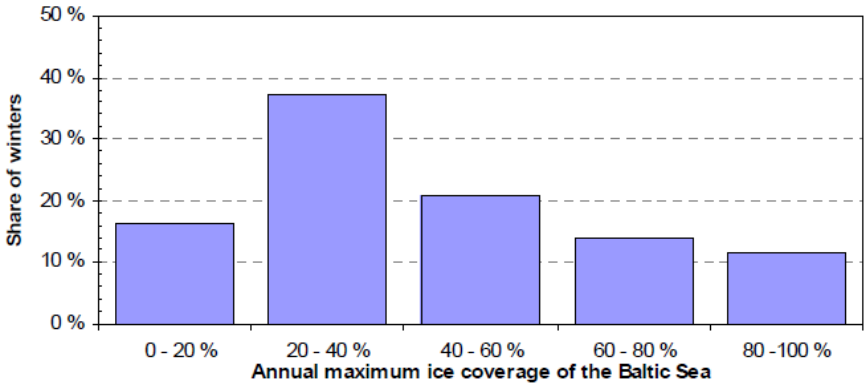

Figure 3 *The annual maximum ice coverage of the Baltic Sea in years 1961-2003presented as a histogram* **[11]**.

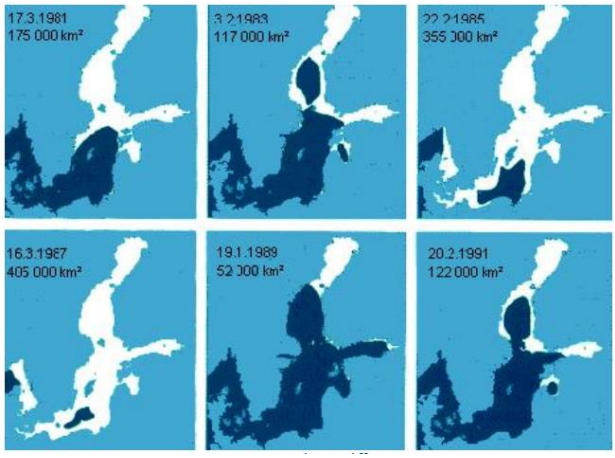

Figure 4 *Maximum ice cover during different years* **[14]**.

In addition, when ship navigates in ice covered area, quantity the ice coverage, which tells how much of the area is covered with ice, is an important for describing ice conditions. If the ice coverage is 5/10 or less, it is possible to navigate in open water around the ice floes. Further, drifting and ridging is characteristic to the Gulf of Finland and it also affects the winter navigation highly. The prevailing westerly winds push the ice east causing heavy ridging in the eastern parts of the gulf. The probability of encountering big ridges increases moving eastwards and also the distance between ridges gets smaller [15].

Further, many things influence on mechanical properties of ice. Therefore, it is difficult to define exactly values for ice properties. The mechanical properties of sea ice depend on several factors. The most important are

- grain size and crystallography orientation
- porosity and salinity
- loading rate
- temperature

One could also pay attention to the geometric scale effects and boundary condition, such as confinement applied during loading [11].

Kujala et al. [16] suggest values that are characteristic for sea ice in the Bay of Bothnia. These values are used in calculations as the most reasonable selection for modeling ice behavior in the Baltic Sea, see Table 1.

Table 1 *Mean ice parameters for the Baltic Sea* **[16]**.

Parameter	Value	Unit
σ_f	580	kPa
σ_c	2 - 4	MPa
ρ_i	900	Kg/m^3
ν	0.3	
E	5	GPa

Ice conditions in the Baltic have been recorded on charts as navigational aid to ship crews for many decades. Before the time of airborne and spaceborne remote sensing, ice charts were based on ship reports and occasional ground truth observations, which provide only limited information. Aerial reconnaissance played an important role until the 1970s, but since then satellite observation technology has been the main source of information [3]. Ice charts are useable in providing information about the ice thickness and floe size. Moreover, Russian ice charts contain information about ice compression that the Swedish and Finnish ice charts are missing. In spite of limitations, ice charts are still in use. They help ship crews to have insight into the ice condition as well as to avoid a ticker ice. An example of the ice chart produced by SMHI is presented in Figure 5.

According to Leppäranta [3] the main problem in sea ice charting is how to obtain good ice thickness information - this is also the main problem for the progress of sea ice dynamics theory and modelling.

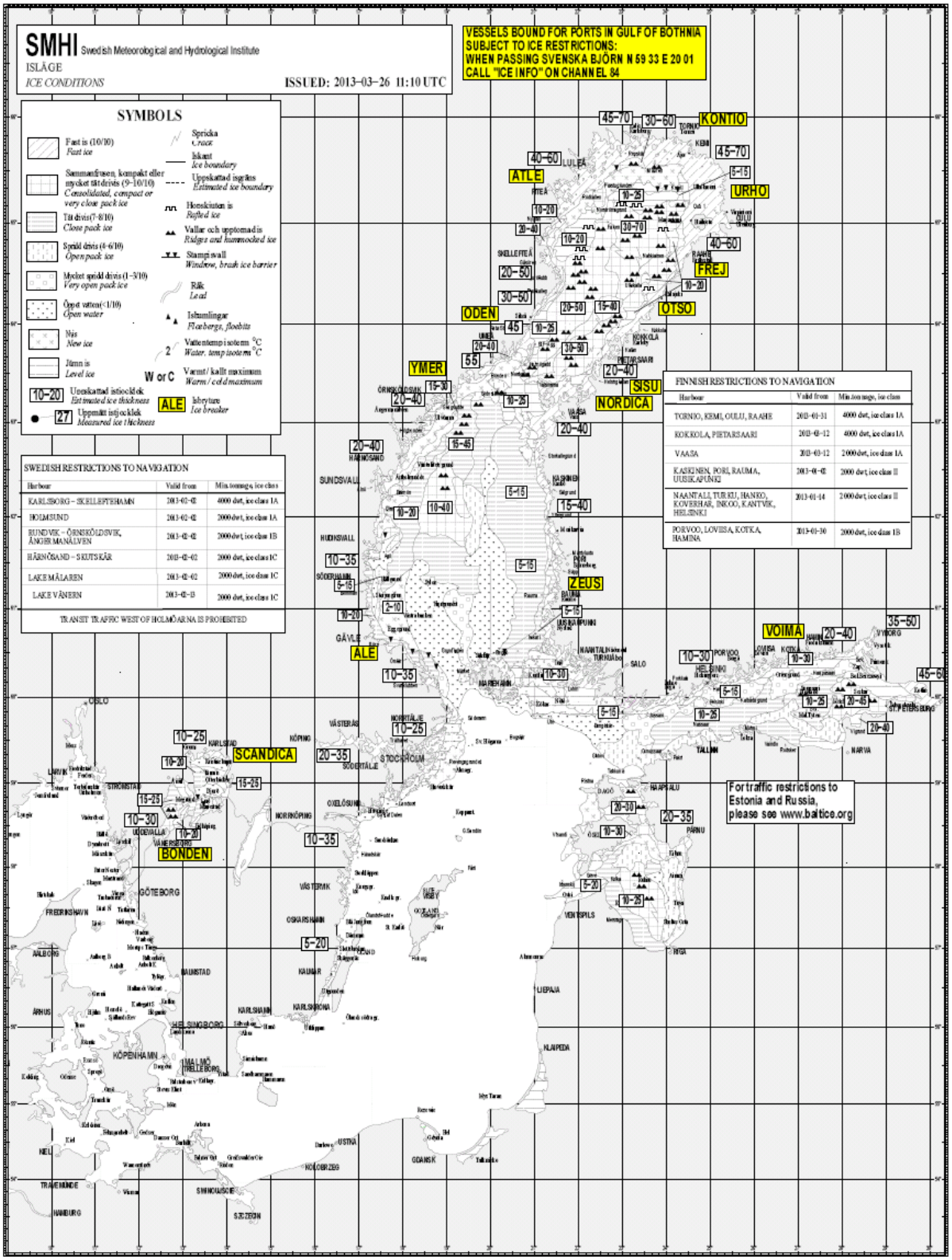

Figure 5 *Ice chart from 26.03.2013, produced by SMHI* **[17]**.

Thin ice can show extreme behavior (Figure 6); due to wind forcing, the whole ice cover in the Bay of Bothnia, Baltic Sea was driven in 6 days into the north-east corner (into an area 20% of its initial value) [3].

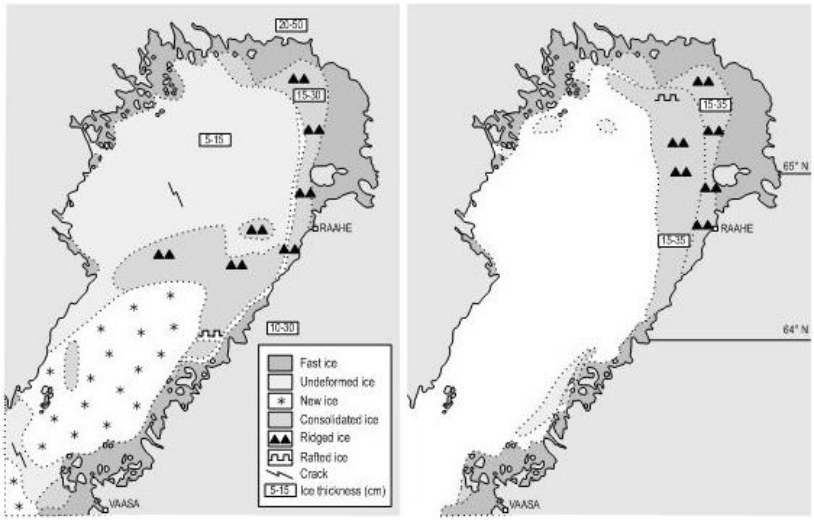

Figure 6 *Ice situations in the Bay of Bothnia on 20 and 26 February 1992. Strong southerly to westerly winds drove the ice to the north-east corner of the basin* **[3]**.

Finnish Meteorological Institute (FMI) [18] presents forecasts of the ice motion and concentration, mean ice thickness, ridged ice thickness, ridged ice concentration, compressive region and deformed ice fraction. The forecasts cover the area of the northern Baltic Sea with spatial resolution of one nautical mile, and range over two days in three-hour steps. Ice parameters are based on products made from satellite data (FMI, Polar View). An example of ice forecasts in the Gulf of Finland on 15.3.2013 at 3:00 UTC is presented in Figure 7. Figure 7 a) ice concentration and motions are presented, b) are described as the percentage of ice cover being compressed at some area.

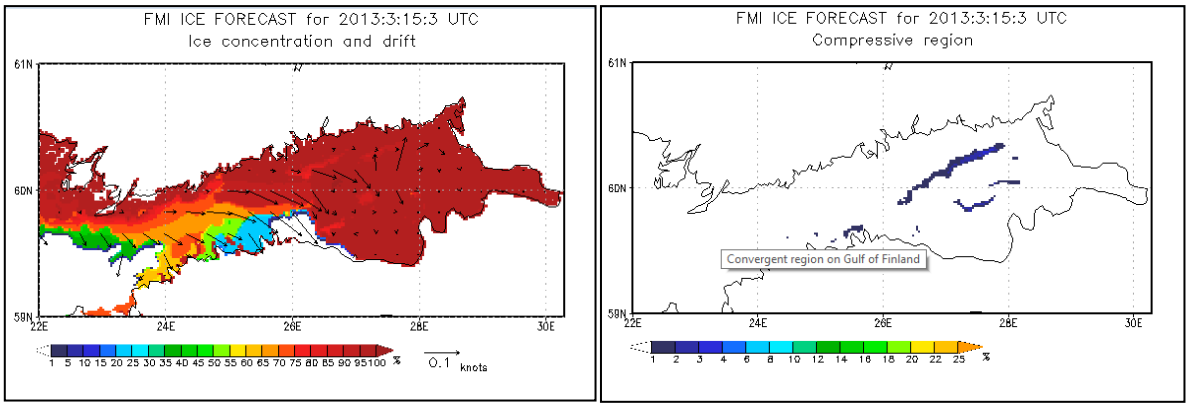

a) Ice concentration and motion *b) Compressive areas*

Figure 7 *FMI ice forecasts for 15.3.2013 at 3:00 UTC* **[18]**.

2.2. Driving forces

Ice compression can be divided into two categories, dynamic and static compression. Dynamic compression is due to wind, tide and current, and the static compression is due to thermal expansion.

In general, the shear stress caused by wind, current or tide on the ice field can be calculated from equation (**1**) where the wind (or current) speed is v, the density of the air (or water) is ρ and the C_D is the drag coefficient

$$\tau = C_D \frac{1}{2} \rho v^2 \quad \textbf{(1)}$$

From the shear stress the force acting on an area of length L and the width b is

$$F = bLC_D \frac{1}{2} \rho v^2 \quad \textbf{(2)}$$

This force has the same direction as wind, current or tide. The driving force can be converted to a line load q along a line normal to the wind/current/tidal direction as

$$q = \frac{F}{b} = LC_D \frac{1}{2} \rho v^2 \quad \textbf{(3)}$$

This line load may be compared with ridging or rafting loads as these are also given as line loads, even if the comparison is not exactly correct as the ridging (or rafting) is driven by the stress in the ice field, not directly the driving stress.

The stress caused by wind depends on the wind speed, direction, duration at the timescale of days or weeks and sea ice surface roughness. In the open seas, where wind speed is dominant driving force, freely drifting sea ice moves at speeds of about 1-3 percent of the wind speed, but when the area is more restricted by shorelines or ice coverage is large, the duration of the wind and the direction become more important. By Leppäranta [3] in the Baltic Sea on average the drift velocity was 2.5% of the wind speed and the direction of the ice drift was 20° to the right of the wind direction. However, the ice velocity experienced some remarkable changes, which cannot be explained by a linear wind drift rule: occasionally, the ice nearly stopped during a moderate wind. This behavior is typical of for drifting sea ice: in general there is a good connection with wind field (or ocean currents), but sometimes the ice takes "unexpected" steps, which are due to its internal friction. Wind drag coefficient for Baltic Sea is about $1.5*10^{-3}$[19] – depending on the roughness of ice surface; roughness that is mainly caused by ridging. The force generated from ocean currents typically acts in the opposite direction of the wind force and therefore it acts as a drag on the wind-driven sea ice motion. Ice-water drag coefficient is about $2.0*10^{-3}$ [3].

2.3. Ridging process

Rafted ice consists of two or more ice layers, of the same ore varying thickness, which have overridden each other (Figure 8). It tends to consolidate quickly into a single thicker sheet,

since only a thin layer of water separates the layer. Rafted ice may also occur at the edge of first-year floes when the ice is thin. Since it is difficult distinguish rafted ice from normal sheet ice, the area the formed can cover has not been well documented [20]. Vaudrey [21] reports that rafted ice of two to three layers is common in the Beaufort Sea, whereas, in the Bering Sea, it can exist in as many as three to six layers.

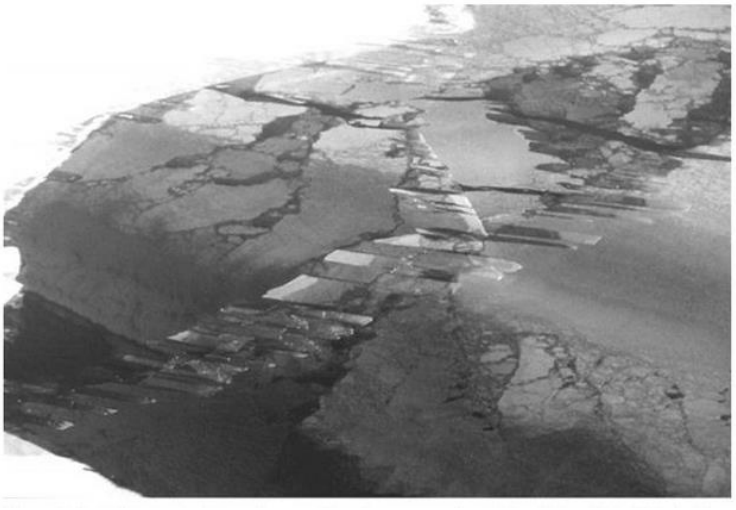

Figure 8 *Thin ice sheets under rafting in compression. The width of the interlocking fingers in the picture varies between 1 and 10 m* **[3]**.

First-year ridges are complex features with widely varying sizes, shapes and properties. This has made their characterization difficult. A ridge is formed when two large ice floes or ice fields collide to each other. The ice field might split into two large ice floes or ice fields collide to each other before or during the compression process [11]. Ridge-building processes are complex, but usually involve some rafting in combination with various bending, buckling or crushing failures. This failure initiates the ridge growth. The resulting ridge feature contains a large number of ice pieces of varying sizes that are piled in a haphazard manner. If the piling continues, the keel may grow as sketched in Figure 9 (c). It can be assumed that with increasing depth of the rubble, higher force is needed to add blocks into the keel [22]. At some stage, when the piling force is high enough, the ice sheet may break at some other location and initiate ridging there, or the keel may start growing laterally to form a hummocked ice field [6].

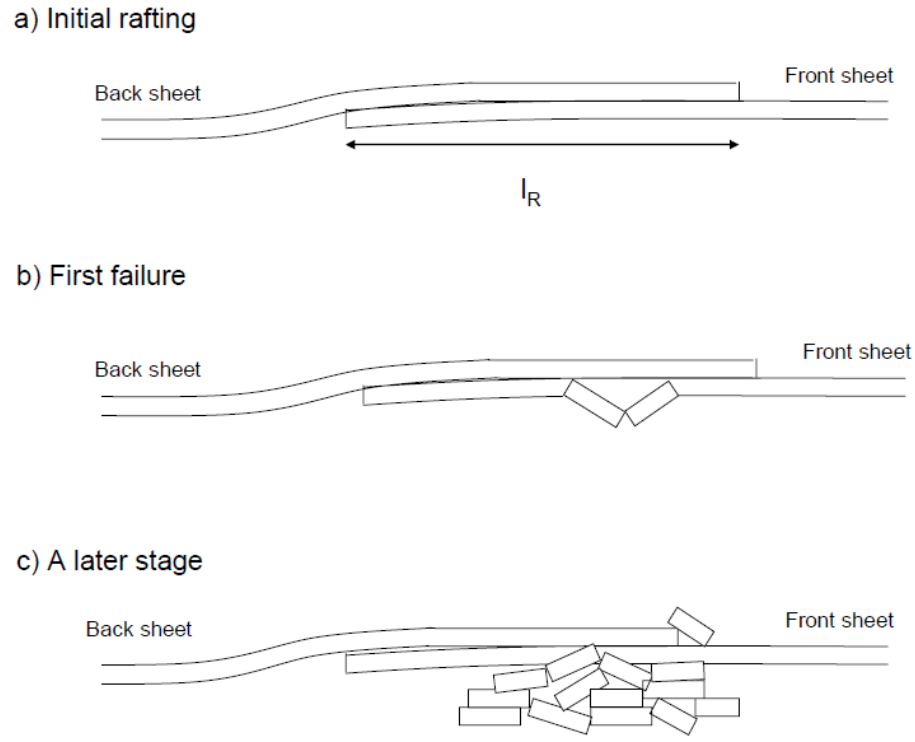

Figure 9 *Cross-section of the different phases of ridging process* **[22]**.

Due to hydrostatic equilibrium, the rubble above the water line (the sail) has a volume of about one tenth of the rubble below water line (the keel). Between the sail and keel it is refrozen zone called consolidate layer as shown in Figure 10. The consolidate layer of the ridges is normally thicker than the level ice and thus the ridges are difficult to penetrate and they form the biggest obstacles for winter navigation. The level ice thickness does not describe the ridges ice field well. For ridge ice field it is possible to calculate the so-called equivalent ice thickness which means the thickness when amount of ice in the ridges would be distributed evenly at the whole area [13]. The main dimensions of a ridge are defined in Figure 10 in witch h_k is the thickness of the keel and h_s is the thickness of the sail. Both of them are measured from the water level. h_i is a level ice thickness and h_{cl} is the consolidate level thickness. FB means freeboard [11].

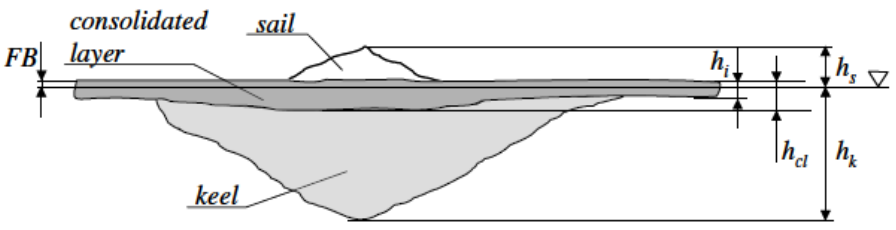

Figure 10 *Main dimension of a ridge* **[11]**.

The values and relationship for ridge morphological parameters have been studied in various regions during numerous field investigations. Timco and Burden[23] presented the following

ratio, equation (**4**), for first-year in which the cross section was approximated with an ideal triangular shape.

$$\frac{h_k}{h_s} = 4.4 \quad \textbf{(4)}$$

According to investigation in the Baltic Sea, Kankaanpää [24], the keel depth is

$$h_k = 6.35h_s - 0.02, \ \text{m} \quad \textbf{(5)}$$

Characterizing consolidate layer, one can define the ration R between consolidate layer thickness and level ice thickness as

$$R = \frac{h_{cl}}{h_i} \quad \textbf{(6)}$$

Høyland [25] observed that consolidate layer thickness measured by thermistor strings was lower then found by drilling. Temperature measurements in Spitsbergen and Marjaniemi in the Gulf of Bothnia indicate R = 1.39 - 1.61 while the drilling gave R = 1.68 - 1.85. The most important reason for the difference was that partial consolidate ice was interpreted as a solid ice in the drilling measurements. However, the growth of consolidate layer did not depend on the investigation method. Høyland [25] also summaries several results from literature and conclude that ratio R is between 1.2 and 1.9.

Another important measure that describes the ridge ice field is the ridge density (ridge/nautical mile). The closer the ridges are the more difficult the ice field is to navigate. The ridge density is usually mentioned in the ice charts and is based on the reports from the vessels navigating at the area [15].

The basic factors controlling the dynamics of ice cover area the floe-floe interaction and ice ridge formation. The basic quantity in ice dynamics modeling is ice thickness distribution. The stresses in the ice cover are described in ice dynamics modeling by line loads q and limit stress when ridge starts to form is of order q_c = 100 kN/m [26].

3. The ship in compressive ice

Sailing in ice covered area need special requirements for ship and crow. The most obviously threats come from the increase loads in the ship hull through ice contacts, but also to the propulsion system and appendages such as the rudder. In this chapter is described phenomena related to ship-ice interaction.

3.1. Compression process on ship

Ship performance in ice consists of ability to sail in ice infested waters, e.g. break ice and to maneuver in ice. Navigating in compressive ice is challenge for ship crews. When sea ice compression occurs, the ice touches the ship sides, the ice resistance increases and if the resistance is larger than the thrust of the ship, the ship stops. If the compression continues, the ice starts to break against the ship's parallel midbody. The loads can be very large; in the Baltic Sea the magnitude of these loads can be 1 MN/m, much higher than the average stresses in compressive ice cover [26]. The force decreases only when the channel has closed completely.

One of the signs of sea ice compression is closing channel behind the ship. In difficult ice conditions, where strong compression occurs, channel closing is easy to detect; the channel edges are pushed together and they might even cause a small ridge or the ice is piling against the ship hull. The difficult comes when sea ice compression is not strong. In these cases the driving force has reached its maximum, which is less than force required for ridging or rafting, and actual motion in the ice field is difficult to observe. The back whirl from the ship causes an effect where sea ice blocks are filling the channel. This effect can easily mislead the observer because the channel looks like it is closing.

The compression is not uniform along the whole hull, and therefore the force tree, which was mentioned earlier, might be a way to approach ship in compressive sea ice field problem. Instead of assuming that the force is only in ice floe edges, the stress is transmitted from flow through the force tree. As can be observed from Figure 11, the ship experiences compression from force tree lines. The ice is piling up against the hull in these points.

Figure 11 *Ship in compressive ice field. Red arrows show the ice piles, which might be caused by force lines in the sea ice field. The vessel entered the area assisted by icebreaker Tor, and the ice piles where created while icebreaker Tor released M/S Eira from ice in January 2010 in the eastern Gulf of Finland* **[6]**.

It is noted that the ship can experience compression even if the wind direction and the ship course are not perpendicular. If the stress tree line-theory is applied, the ship can experience compression, but the compression might not be as high as in the case where the stress lines are perpendicular to the hull. If the ship course is parallel to wind stress, and therefore parallel to compression, the ship hull is not expected to experience any compression [6].

3.2. Scaling

Compression in a sea ice field can be observed in different scales. Ice engineering has focused on the local scale (1-10 m), while in geographical sea ice dynamics, the scale of the interest have been meso-scale to large scale (100-1000 km). These models describe the compression in selected sea ice areas and the theory used in the models is based on continuum physics. But in the ship scale, much smaller than 1000 m, the compression is considered to be very local. Even along the length of ship hull, the compression can vary significantly. Measurements show a large scatter of values for the local area because of the stochastic nature of the ice. The local force acting on the vessel is much larger than the large scale compressive force. The local strength is in the order of 1-10 MPa, while the meso-scale strength is 10-100 kPa in compact ice. Figure 12 presents Sanderson's curve, gives a rough idea how stress behaves as a function of the size of the loading area. Results from laboratory tests to a large-scale drift ice models are included [3].

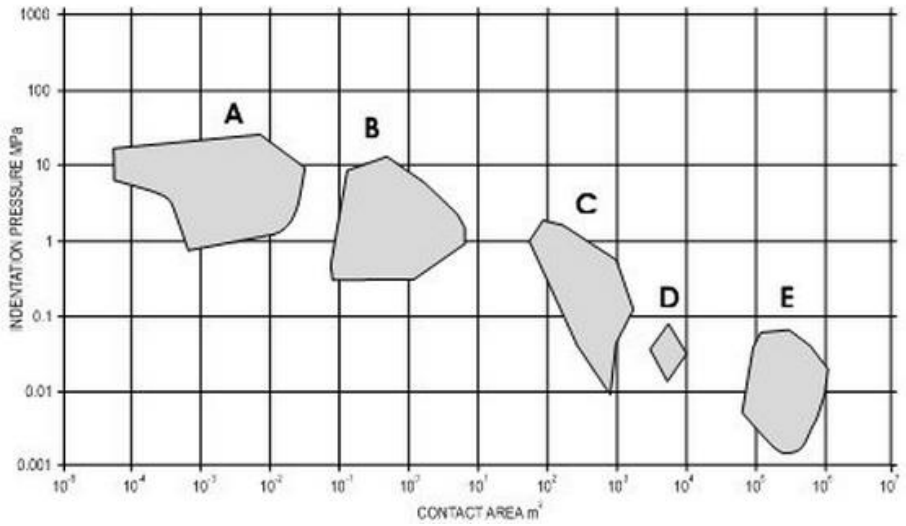

Figure 12 *Sanderson's curves: the strength of the sea ice vs. the loading area. A to C show local-scale tests, D shows Baltic Sea high-resolution ice drift models, and E shows Artic Ocean meso-scale ice drift models. From* **[27]**, *but with Baltic Sea drift ice data (D) added.*

Several observations have shown that the ice line load i.e. load per unit horizontal width depends on the length. Figure 13 depicts some results from ship born measurements. All these measurements suggest a form of

$$q = C * L^{-0.7}, \qquad [L] = \text{m} \tag{7}$$

for the measurement results. The constant C varies a bit, but for the Baltic the result of maximum ice forces from IB Sisu measurements would be most suitable – here C = 1310 kN/m (when lengths are given in m). This scaling results in ship scale to a value q = 39 kN/m (L = 150 m) and in the scale of ice dynamics 6.8 kN/m. The latter value corresponds to a total force of 1250*10^4 N which compares well with the maximum compression values calculated [4].

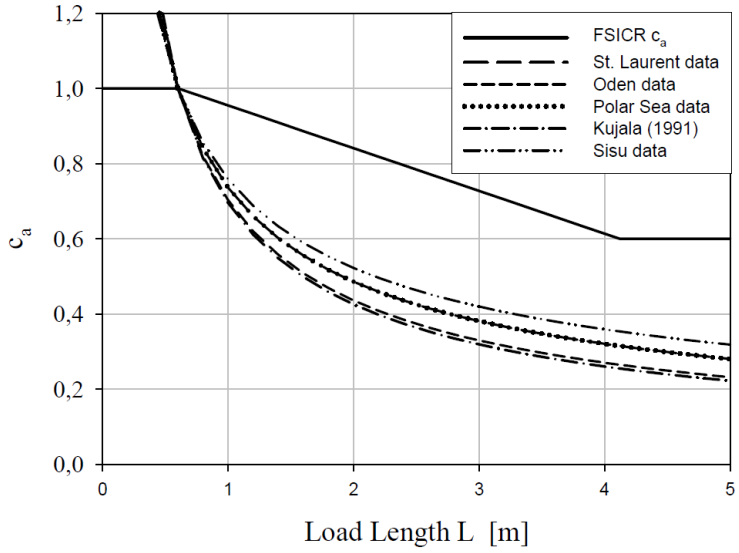

Figure 13 *The dependency of the line load on the contact length in various ship borne measurements scaled so that they all are one when L = 0.6 m* **[4]**.

In consequence, the relationship between the ice stress on the geophysical scale and the ice engineering forces is highly complicated, and there is no easy way for downscaling or up-scaling. This is one of the key problems in sea ice mechanics nowadays and not solved yet.

3.3. Loads on ship hull caused by compressive ice

Two types of ice behavior are assumed to occur in the beginning when an ice sheet contact with (vertical) ship hull; crushing and flaking. When the contact is with the vertical ship hull, the crushing is ideal. Under sufficient load, a flake is formed from the contact area to the ice edge. When the flake is formed, the contact width and the force are decreased. When the compression persists, ice sheet continues to move and the force builds up again. Each flake also results new ice block geometry. This model is given in [28]. Figure 14 shows an idealized sketch of the contact between a large ice feature and a structure. All items except the flexural crack will be present in every ice contact, though to varying extents.

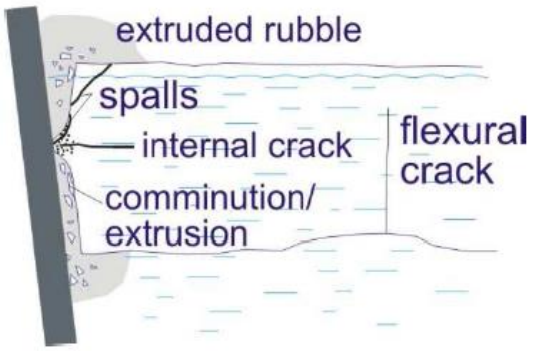

Figure 14 *Sketch of ice contact with a structure* **[29]**.

When the ice meets ship hull the following failure processes are present:

- Local crushing of ice cover near the ship
- Pile up (and down) of crushed ice
- Bending failure of the ice cover
- Ice pile-up formation against the ship (Figure 15) or formation of ridges [30].

Figure 15 *The ship is in compressive ice field where the ice has piled against the ship hull (Pentti Kujala)* **[6]**.

Although the failure process is complicated, the crushing may be presented as a simple contact model. When the crushing proceeds, the force builds up and drops in a sequence of triangular peaks. Wide range of different size of flakes is resulted for cracking pattern. High peaks in force are related to large cracks which produce larger flakes. The cracks tend to form at specific angles, dependent on the direction of the edge to which they run.

Further, while the ice is crushed, the contact increases, also the total force increases. The contact situation proceeds by crushing till the force is great enough to create bending fracture. Bending can therefore also occur in vertical midbody, but only when the piles generated from crushing are large enough. Bending failure process can be identified from triangular or circle sectors shaped ice floes next to the ship, see Figure 16 [6].

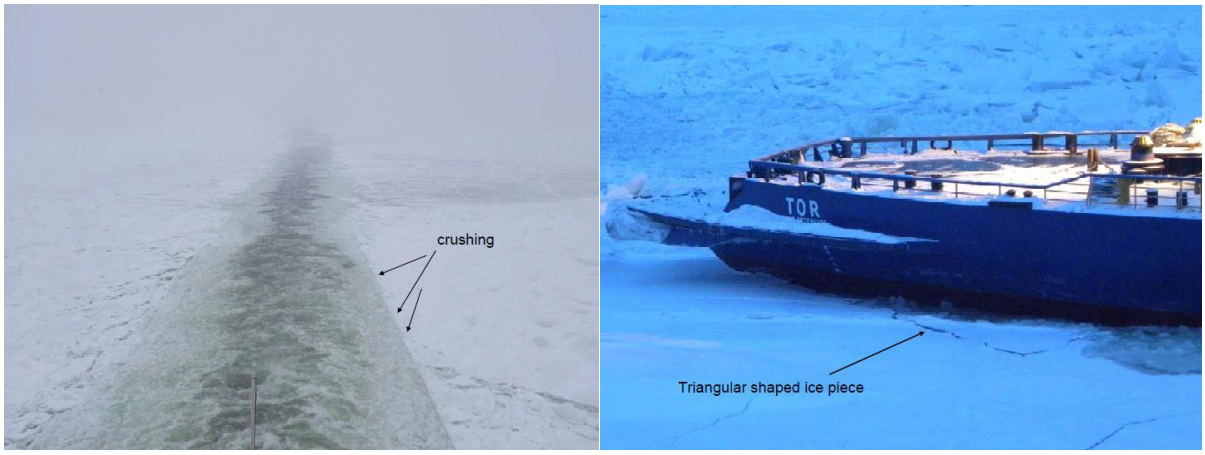

Figure 16 *The edge of the channel has been broken by crushing (right). The ship is reversing. The black arrow shows the triangular shaped ice piece, which form due to bending (left)* **[6]**.

Development of the ice compression against the ship side model was discussed based on the observations made in the joint research project between Institute for Problem in Mechanics, Russian Academy of Sciences and the Ship Laboratory at Helsinki University of Technology about ships in compressive ice [1]. The ship-ice compression process is sketched in the Figure 17. Interaction between the ship and the ice begins with local crushing of ice when the ice hits the ship (Figure 17, from *a* to *b*). Crushing creates piles of ice on top and bottom of the ice. Crushing continues till an ice floe is broken from the ice field because of bending or buckling failure (c). In this point of the process, the ice plate is bent upwards or downwards, and the process starts again with local crushing (d) [6].

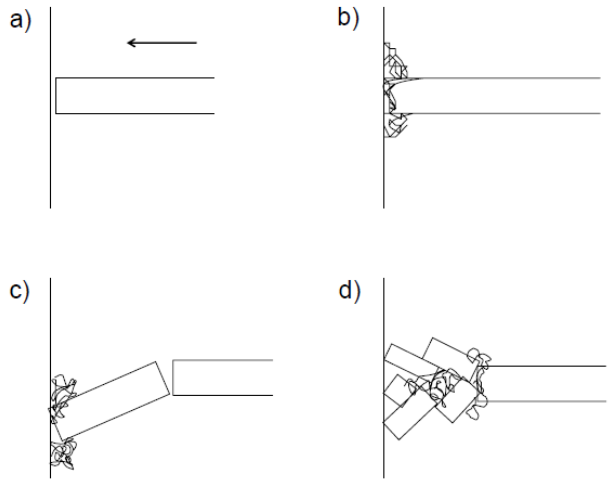

Figure 17 *The sketch of ship-ice compression process. At first, the ice is moving towards the ship (a). Interaction between the ship and ice starts with local crushing of the ice (b). Crushing continues till the sector of ice is separated from the ice field because of bending or buckling failure (c). The sector is bent upwards or downwards, and the process starts again with local crushing (d)* **[6]**.

Definition of ice loads under the compression consist different variable. Kendrick [31]defines the ice pressure scenario. The parameters dictating the total load level are:

- Ice thickness;
- Ice bending strength;
- Hull geometry;
- Driving forces.

The first three parameters will set the upper bound on the load which the ice can sustain without failing. At the local level Kendrick [31] lists other important factors which affect the overall load distribution along the ship structure:

- Ice floe/piece size;
- Ice crushing strength;
- Structural elasticity.

The ice pressure in the ice sheet will result from driving forces, limited in certain load-carrying capacity of the ice cover. The limit can be determined for each ice type. The line load (kN/m) can be expressed as

$$q = 100{h_T}^{1,25} \quad \textbf{(8)}$$

where the $h_T$is the characteristic ice thickness.

3.4. The Russian system to identify sea ice compression

Scientists from Russian Institute of Problems in Mechanics use this method to rank compression in the area. Crew observes and estimates length of open water channel behind the ship. Basics of the method are presented in the Figure 18. If the channel stays open for one nautical mile or more behind the ship, there is no compression. On the other extreme, if the channel closes immediately after the ship and pressure ridge is formed where the channel used to be, compression can be ranked as very strong compression or with grade 3. This kind of method cannot be very accurate, as it depends on the variables such as experience of the crew making the estimation, type of the ice, fog, ship speed and the breath of the broken channel behind the ship.

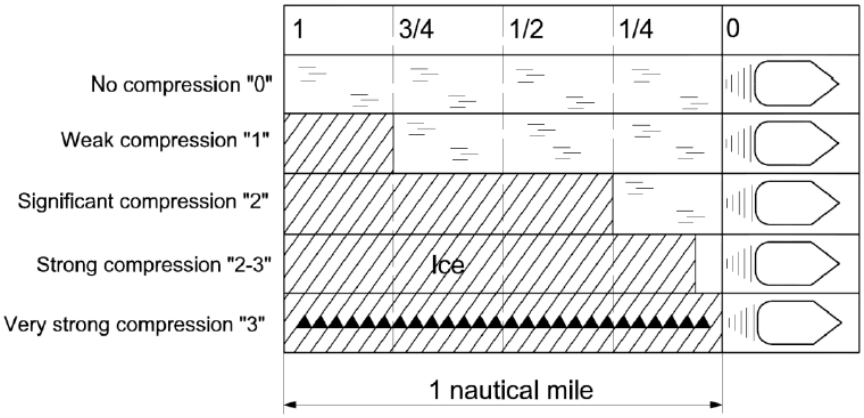

Figure 18 *Russian compression grading system* **[32]**.

3.5. Ice load measurements

The largest concern for the shipping safety in such ice-covered waters is the load on ship hulls from surrounding ice. Generally, ice load depends on many parameters such as hull form, ship operation, ice conditions etc. Full-scale measurement is the most commonly used and also reliable way to study the problem of ice loading on ship hulls. However, full-scale measurements rare because they are expensive and time consuming. In the text below is briefly described measuring equipment and results from IB Sisu and MS Arcturus.

IB Sisu

Full-scale ice load measurements in the Baltic Sea have been done on icebreaker Sisu from 1979 to 1985. The measurements on Sisu included short term and long term measurements. The analysis of the short-term measurements were based on the peak amplitude distribution, instead the long-term measurements were based on the measured daily maxima. Instrumentation onboard IB Sisu was expanded in phase during 1982-84. The final configuration had 4 gauges for ice pressure on plating, 4 stress strain gauges on plating, 3

single strain gauges on frame flanges, 1 shear strain gauge pair in a stringer, and 22 shear strain gauges in the webs of 10 frames. Maximum pressure was 11.5 MPa, maximum load on frame 2050 kN/m and maximum total load 1825 kN. Loading events had duration from 20 to 600 milliseconds. The measured speed of IB Sisu varied, but is mainly in the range from 10 to 13 knots. The maximum ice thickness in the Bay of Bothnia during 1985 varied from 1.07 to 1.10 m with high probability of ice ridges and rafts. Layout of the instrumentation is shown in Figure 19.

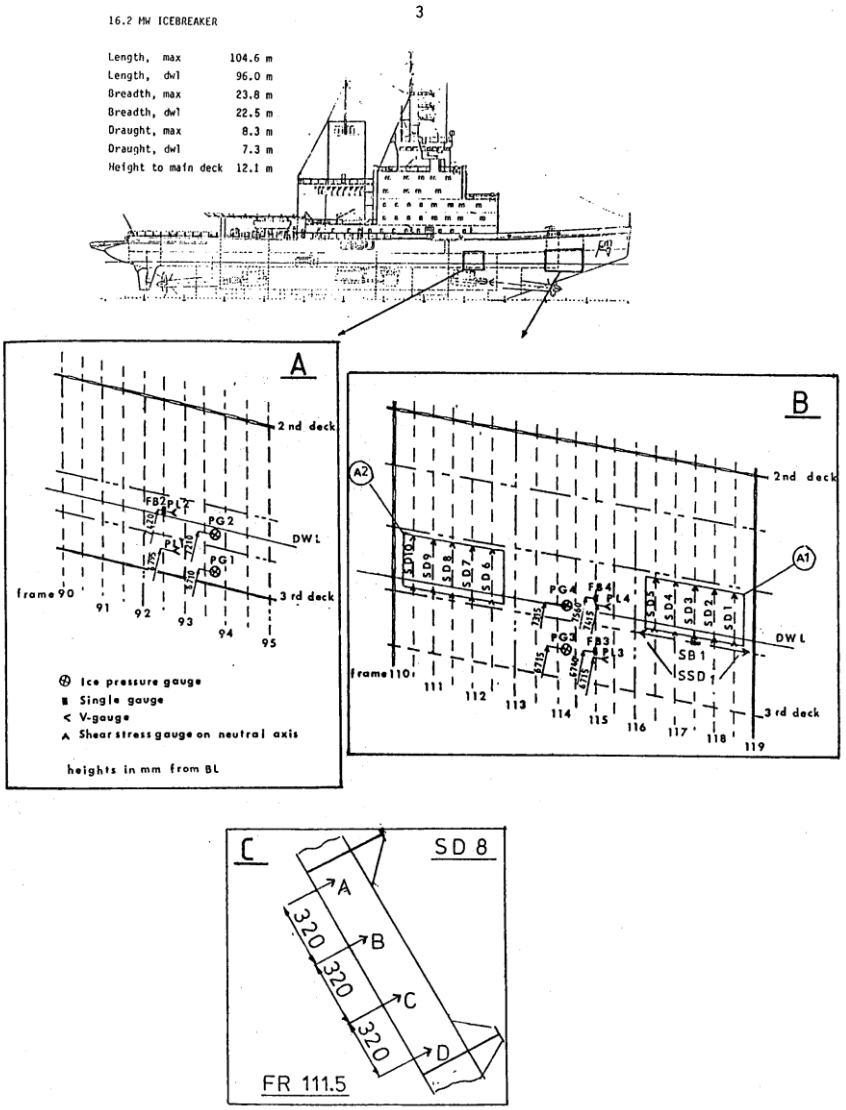

Figure 19 *Layout of the instrumentation onboard IB Sisu* **[33]**.

MS Arcturus

MS Arcturus is a 13090 DWT Ro-Ro vessel, which navigates from Helsinki, Kotka, and Hamina to Central Europe. The Baltic ice class of MS Arcturus is 1A Super.

Long-term ice loading measuring program onboard MS Arcturus was conducted during winters 1983-1988. The hull instrumentation consists of 4 ice pressure sensors, 6 strain gauges for plate and frame responses and 20 shear strain gauges for frame ice loads, see

Figure 20. The main navigation area in ice for MS Arcturus is the Gulf of Finland. The maximum load acting on one frame was 1190 kN/m and the maximum ice pressure was 6.7 MPa.

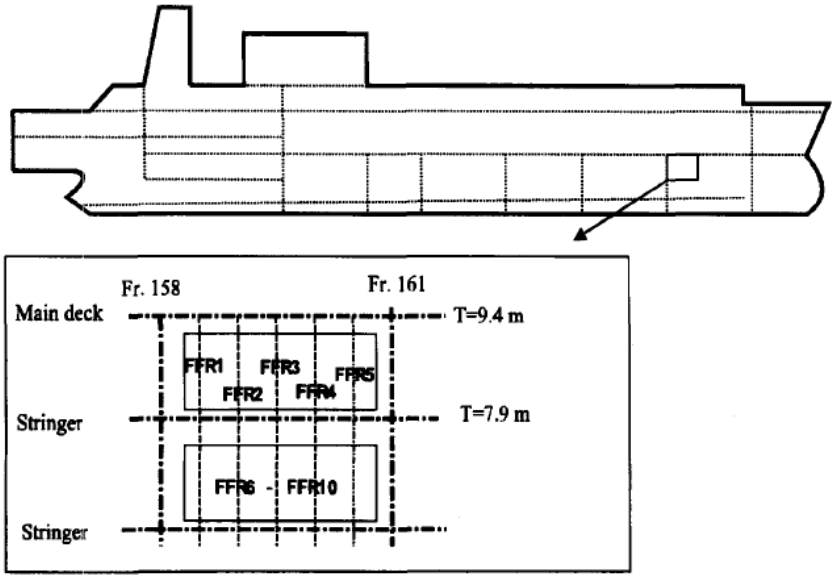

Figure 20 *Layout of the instrumentation at the bow of MS Arcturus* **[34]**.

3.6. Ship damages

A hull rupture of tankers in compressive ice would lead to catastrophic consequences in the Baltic. For example, if the structural integrity of one AFRAMAX size tanker were lost due to high ice loads, and all of its cargo was discharged into the Baltic Sea, the mean total cost expected would be 1240 M€ [35]. Figure 21 illustrates the damage caused by the ship-ice interaction.

Figure 21 *Damaged areas caused by ship-ice interaction* **[36]**.

The identified hazards of winter navigation are based on earlier studies, see for example Kujala [37] and Juva [38]. Within SAFEWIN project, in winter 2010 was recorded that 63 ships stuck in the ice and they were in need icebreakers assistance. Some of the ships were caught in ice twice [39]. Furthermore, at the same day 10 ships were in the same area, as the ships presented earlier, but did not need any icebreaker assistance. It is noted that these ships had some difficulties.

Hänninen [36] was studied ship damages in winters 2003 and 2004. The total number of ice related incidents recorded in the study was 98, and the number of ships involved was 111. The number of ship is larger than the number of accident because in some cases two ships were involved in the same incident. Crew report from oil tanker and tug boat describe scenario when ship stuck in converting ice.

Report: 95000 DWT Oil tanker, ice class IC

The ship was caught in ice near Suursaari on the 11th of January 2003 of her way from Russia to Denmark. During the compression event, the ice blocks piled up against the SB side of the ship. The plating in the midship area got permanent deflections in the area of two frame spacing for a length of about 100 m. The maximum indents were about 30 mm. The draught was 14 m and the damaged area was about 1.5 m below the waterline.

Report: Tugboat, ice class IA

The ship was damaged in the Gulf of Finland 21st of January 2003, because the sea ice field was moving, and it was converging. Eventually, the ship was caught in ice, and started drifting sideways along the ice masses with a speed of 2-3 knots. In the compression, the ice started to pile up against the ship's side shell. Pile-up and drifting lasted about 20 minutes and after that ice pieces started slide below the ship bottom. When the compression decreased the ship drove to the fast ice and waited for icebreaker assistance. An icebreaker towed the vessel to the nearest harbor.

The ship damage, in both cases, happened close to the high growth rate of deformed ice at the interface of different ice conditions with notable ice thickness gradients [40]. Generally, ridging and rafting areas are considered as major risk region for ships navigating in sea ice field. In the analysis of the incident area, large compressive forces occurred fairly far from the intense compression regions. According to the finding, the ice compression is very local event and navigation channels/leads can initiate ridging with relatively low compression rates [40].

4. MODEL TESTING

Ice model testing is typically used to estimate a ship's performance in ice in the design stage. There are 12 ice model testing tanks in the world, out of which two are in Finland. One is at Aker Arctic and the other at Aalto University. Usually the model test focuses on investigating only one phenomenon at the time, for example, level ice resistance, ice channel resistance or ice ridge resistance. When modeling, several phenomena acting on the ship model need to be taken into account in the analysis [10].

The test program of the SAFEWIN testing included six test series with varying ice thickness and compression levels. The model was fitted with measuring equipment that enabled the registration of resistance, ice loads and ice pressure on the bow shoulder and the parallel midship during testing. Further, the force added to the ice sheet by the pusher plates was measured with load sensors on them. The test layout is presented in Figure 22.

The tests within SAFEWIN project were conducted in the ice basin of Aalto University. The sides of the basin are 40 meters and the depth is 2.8 meters. The model ice in the basin is granular ice of ethanol solution [41], produced by spraying droplets of the water-ethanol solution into cold air, which then cool and drops onto the surface of the basin, forming slush ice. This procedure is continued until target ice thickness is reached. After spraying, the ice properties are achieved by tempering the ice cover where the temperature is decreased below -15 °C and then measured properties of the ice cover.

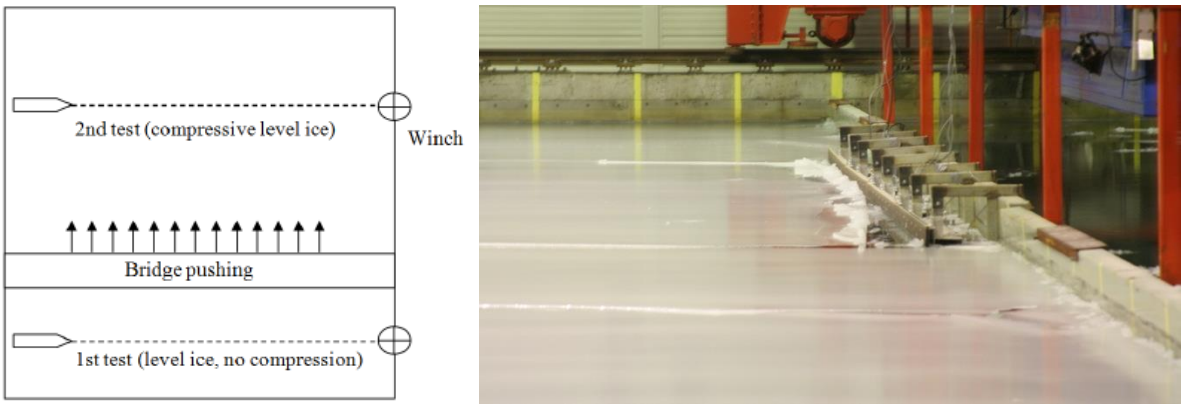

Figure 22 *Layout of the test arrangement (left) and the pushing plates lowered to the water level (right), modified* **[8]**.

4.1. Test preparations

Before testing, it is necessary to calibrate and set up measuring equipment, as well as determine the properties of ice. Furthermore, ice thickness, bending and compressive strength, elastic module and friction between ship model and ice have to be measured.

The properties of the ice sheets play an important role in the tests. Ice properties are measured more times in different positions. Figure 23 presents an example of location and hole where the ice properties were measured. The mean value is used in further analysis of test results. Moreover, to satisfy both the Froude and Cauchy scaling laws, ice properties; the elastic

module E, the flexural strength σ_f and compressive strength σ_c have to be linearly scaled using the scaling factor λ, see e.g. [42]. The fine-grained structure makes the model ice as such much more homogeneous and isotropic than natural sea ice, but some variations in the properties are still encountered [7].

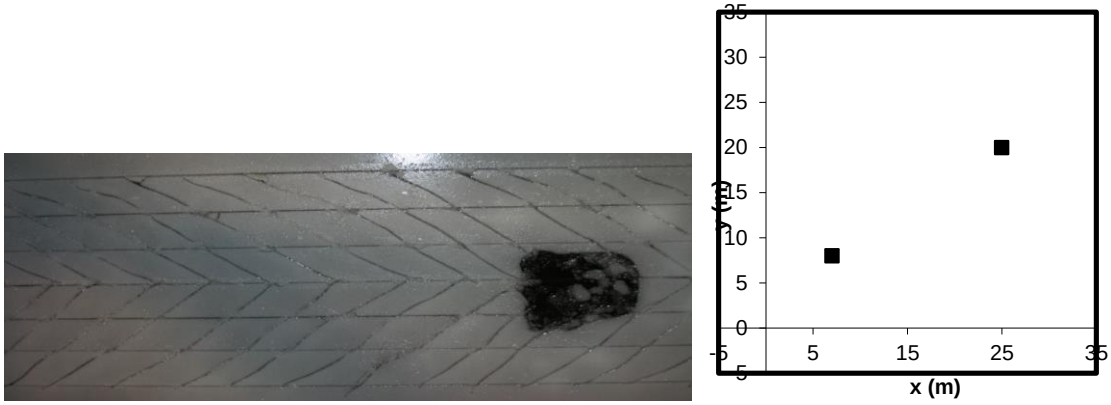

Figure 23 *Pre-sawn ice field, the hole shows a location where the ice properties were measured before the pre-sawn ice field was created (left)* **[10]** *and example of location of measuring positions (right).*

4.2. Scaling of model test and ice properties

Scaling is important as the calculation methods applied for full-scale evaluation. The model ice properties were measured before each test series to verify the suitability for model testing and also to obtain a reference to full-scale ice properties. Geometrical similarity scaling was applied for model and the scaling factor derives from the ship model (λ=25). The scaling relations for different variables are presented in Table 2. Table 3 displays the ice measured properties for different test series in a model- and full-scale.

Table 2 *Scaling of different properties in ice model testing* **[43]**.

		Units			**Units**
Length	$L_{FS}=\lambda * L_m$	m	Ice strength	$\sigma_{FS}=\lambda * \sigma_m$	kPa
Time	$t_{FS}=\lambda^{0.5} * t_m$	s	Ice thickness	$h_{FS}=\lambda * h_m$	m
Velocity	$v_{FS}=\lambda^{0.5} * v_m$	m/s	Elastic modulus	$E_{FS}=\lambda * E_m$	MPa
Force	$F_{FS}=\lambda^3 * F_m$	N	Density	$\rho_{FS}=\rho_m$	kg/m^3
Friction	$\mu_{FS}=\mu_m$	-	Acceleration	$a_{FS}=a_m$	m/s^2

Table 3 *Thickness and mechanical properties of ice***[10]**.

Test series number	Model Scale				Ship Scale			
	Thickness [mm]	**σ_b [kPa]**	**σ_c [kPa]**	**E [MPa]**	**Thickness [m]**	**σ_c [kPa]**	**σ_b [kPa]**	**E [MPa]**
1	40	30.8	61.5	51	1	1537.5	770	1275
2	29	29.9	50.5	36.75	0.575	1262.5	746.25	918.75
3	23	22.3	74.3	10.4	0.725	1856.25	556.25	260
4	29	29.7	70.7	64.35	0.725	1767.5	741.25	1608.75
5	29	29.5	56.5	65.3	0.725	1412.5	736.25	1632.5
6	24	22.9	69.9	63.15	0.6	1747.5	571.25	1578.75

4.3. Ship model

The model adopted in the tests was a 21 300 DWT bulk carrier named Credo. It has an ice class of 1A Super of the Finnish-Swedish Ice Class Rules with a bulbous bow, a high block coefficient and a long parallel midship section. The scale of the model is 1:25. The model was prepared without the iceknife, which is visible in the photograph on the Figure 24. Dimensions of the model are displayed in Table 4.

Table 4 *Dimensions of the ship and model* **[10]**.

	Full-Scale	unit	Model-Scale	unit
L_{OA}	159	m	6.36	m
L_{PP}	148	m	5.92	m
B	24.6	m	0.984	m
D	13.5	m	0.54	m
T	8.75	m	0.35	m

Figure 24 *Bulk carrier Credo* **[10]**.

4.4. Test procedure

The first test of each series was a level ice test without compression. The model speed in all the tests was 0.5 [m/s], which corresponds to 2.5 [m/s] or 4.86 [knots] in full scale. The second test was made in compressive level ice, where the bridge was pushing the ice at approximately 0.002 [m/s]. The procedure in closing channel tests was similar to the compressive level ice test. The bridge started to close the channel by pushing the ice sheet between the model and the bridge, see Figure 1. Ice sheet was crashed on sides of the basin, so that ice was able to drift free. The towing continued until the model reached the other side of the basin. In closing channel tests, different closing speeds were applied to simulate different compression levels. Closing speeds of 0.01, 0.02 and 0.03 m/s allowed to simulate

low, moderate and severe compression, respectively. Closing compressive channel tests were repeated until the ice sheet between the bridge and the channel was broken and unusable. Open channel tests were conducted after closing channel tests. The test programme consisted of six test series with varying ice thickness and compression levels. Compressive level ice and closing channel tests are discussed as a part of this study; other tests are not in the focus of the study, so they are not described, see Table 5 - Table 10.

Table 5 *Conditions in test series 1, modified* **[8]**.

Test #	Ice Description	Ice Thickness	Ice Speed	Russian level
1_2	Compressive level ice	0.04m (1m ship scale)	0.002 m/s	N/A
1_3	Closing channel	0.04m (1m ship scale)	0.03 m/s	3
1_4	Closing channel	0.04m (1m ship scale)	0.03 m/s	3
1_5	Closing channel	0.04m (1m ship scale)	0.03 m/s	3

Table 6 *Conditions in test series 2, modified* **[8]**.

Test #	Ice Description	Ice Thickness	Ice Speed	Russian level
2_2	Compressive level ice	0.029m (0.725m ship scale)	0.002 m/s	N/A
2_3	Closing channel	0.029m (0.725m ship scale)	0.03 m/s	3
2_4	Closing channel	0.029m (0.725m ship scale)	0.03 m/s	3
2_5	Closing channel	0.029m (0.725m ship scale)	0.03 m/s	3
2_6	Closing channel	0.029m (0.725m ship scale)	0.03 m/s	3

Table 7 *Conditions in test series 3, modified* **[8]**.

Test #	Ice Description	Ice Thickness	Ice Speed	Russian level
3_2	Compressive level ice	0.023m (0.575m ship scale)	0.002 m/s	N/A
3_3	Closing channel	0.023m (0.575m ship scale)	0.03 m/s	3
3_4	Closing channel	0.023m (0.575m ship scale)	0.03 m/s	3
3_5	Closing channel	0.023m (0.575m ship scale)	0.03 m/s	3
3_6	Closing channel	0.023m (0.575m ship scale)	0.03 m/s	3

Table 8 *Conditions in test series 4, modified* **[8]**.

Test #	Ice Description	Ice Thickness	Ice Speed	Russian level
4_2	Compressive level ice	0.029m (0.725m ship scale)	0.02 m/s	2
4_3	Closing channel	0.029m (0.725m ship scale)	0.01 m/s	1
4_4	Closing channel	0.029m (0.725m ship scale)	0.01 m/s	1
4_5	Closing channel	0.029m (0.725m ship scale)	0.02 m/s	2
4_6	Closing channel	0.029m (0.725m ship scale)	0.02 m/s	2

Table 9 *Conditions in test series 5, modified* **[8]**.

Test #	Ice Description	Ice Thickness	Ice Speed	Russian level
5_2	Compressive level ice	0.029m (0.725m ship scale)	0.002 m/s	1
5_3	Closing channel	0.029m (0.725m ship scale)	0.01 m/s	1
5_4	Closing channel	0.029m (0.725m ship scale)	0.01 m/s	1
5_5	Closing channel	0.029m (0.725m ship scale)	0.02 m/s	2
5_6	Closing channel	0.029m (0.725m ship scale)	0.02 m/s	2
5_8	Closing channel	0.029m (0.725m ship scale)	0.03 m/s	3
5_9	Closing channel	0.029m (0.725m ship scale)	0.03m/s	3

Table 10 *Conditions in test series 6, modified* **[8]**.

Test #	Ice Description	Ice Thickness	Ice Speed	Russian level
6_2	Compressive level ice	0.024m (0.6m ship scale)	0.002 m/s	1
6_3	Closing channel	0.024m (0.6m ship scale)	0.01 m/s	1
6_4	Closing channel	0.024m (0.6m ship scale)	0.01 m/s	1
6_5	Closing channel	0.024m (0.6m ship scale)	0.02 m/s	2
6_6	Closing channel	0.024m (0.6m ship scale)	0.02 m/s	2
6_8	Closing channel	0.024m (0.6m ship scale)	0.03 m/s	3
6_9	Closing channel	0.024m (0.6m ship scale)	0.03 m/s	3
6_10	Closing channel	0.024m(0.6m ship scale)	0.04 m/s	4

The level 4 compression is an addition to the Russian defined grading system to simplify the analysis of the initial SAFEWIN testing [8].

4.5. Measuring equipment

Ice loads on the bow shoulder and the midship area were measured with load sensors and pressure foils. In order to measure ice loads with load sensors, two panels were cut out from the model and instrumented with load sensors, hereafter referred as load panels. The dimensions of the load panels were 0.3 m * 0.2 in midship area and 0.12 m * 0.2 m at bow shoulder. The centerline of the load panels in vertical direction was at the water line. The pressure foils were then fixed with tape on top of the panels. Figure 25 presents the locations of the load panels and pressure foils.

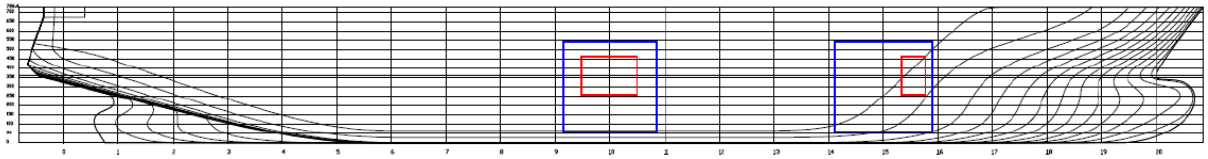

Figure 25 *Locations of load panels and pressure foils. Red rectangles represent load panels and blue rectangles pressure foils* **[44]**.

The midship load panel was equipped with three one-axial sensors which were oriented to measure the normal force acting on the hull surface. Installed load panel at the bow shoulder was equipped with a tri-axial load sensor which measured loads in x-, y- and z-directions. As can be seen from Figure 26, all load sensors were mounted between the panels and supporting structure inside the model [44].

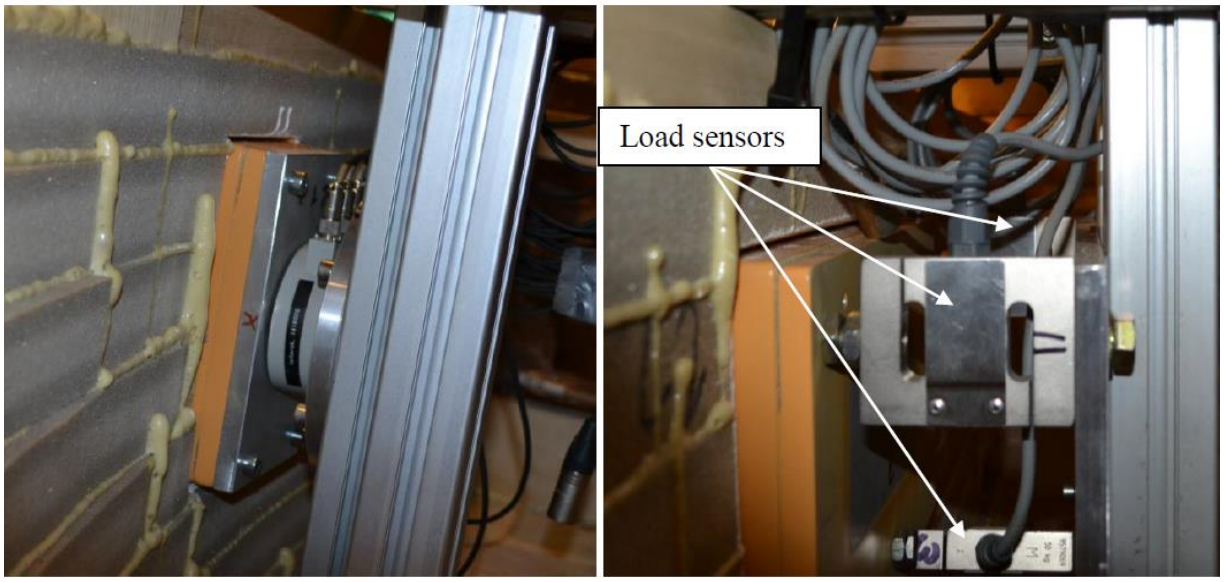

Figure 26 *The load panel at the bow shoulder instrumented with three-axial load sensor (on the left) and the load panel at the midship instrumented with three one-axial load sensors (on the right)* **[44]**.

The pressure foils used in the tests are part of tactile sensor system called I-SCAN. The system consists of a sensor sheet, handle and measuring PC. The sensor sheet used in the tests is model 5350N, see Figure 27. The width of the measuring area is 439.9 mm and the height is 480.1 mm having 44 pressure cells to horizontal direction and 48 to vertical direction. The elements of the pressure foils have voids between each other. Due to the voids, the actual measuring area of the pressure foil is 64% of the total element area. Before fixing the sheets to the model, the sheets were calibrated with dead weights at the temperature of 0˚C. The data from pressure foils are not considered.

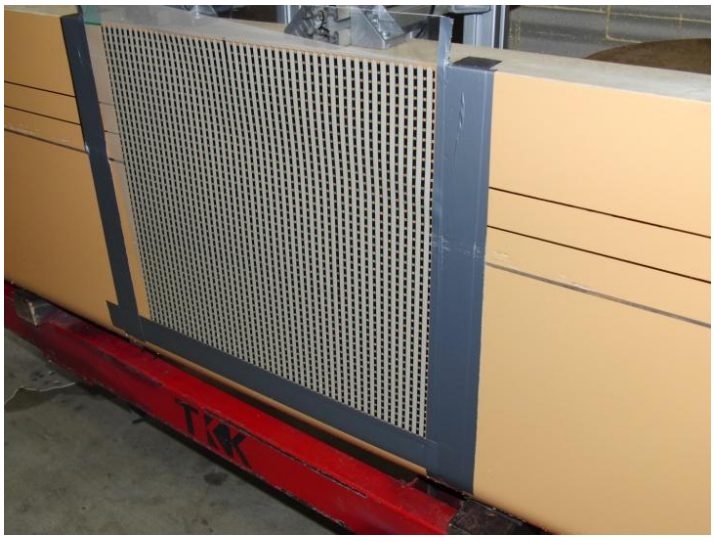

Figure 27 *Sensor sheet taped on the model side* **[44]**.

The bridge above the basin has pushing plates which extend through the whole length. In order to measure the force applied to the ice sheet, a 10 m section of the pushing plates were instrumented with load sensors, see Figure 22. Load sensors were placed in front of the pushing plates. To protect and distribute the load evenly, plates were laid in front of the load sensors. These plates were connected with hinges from above. Altogether 4 plates with breadth of 2.4 m were used, and two load sensors were installed on each plate.

5. RESULTS FROM THE TESTING

The effect of the ice thickness and the level of compression (ice speed) to the ice loads on the model's hull are studied in this chapter. Used measurement data is gathered from the load panels at the midship, bow shoulder and load sensors from the pusher plates.

5.1. Analysis

Throughout analysis, it is assumed that ice is a homogenous solid, and that force transfers evenly throughout the sheet. Also, as the separate pusher plates acting on ice across the entire basin, it is assumed that the line load is uniform along the contact.

Line loads for separate pushing plates are determined by adding up the force measured with the two load sensors mounted on the same pusher plate and then the force is divided by 2.5 meters, see equation (9). It is assumed that the adjacent pusher plates carry the loading over the gap between the plates as the ice sheet is not broken. The pusher plates, forces and line loads are numbered starting from the closest one to the starting point of the test. Line loads are numbered considering how much force is included. For instance Q_{12} represents line load for pusher plate 1 and contains the sum of the forces F_1 and F_2 divided with 2.5 meters, Q_{14} contains sum of the forces F_1, F_2, F_3, and F_4 divided with 5 meters and represents line load for pusher plates 1 and 2, etc. Figure 28 presents an example of the measured time histories with the loads during the same test as presented in Figure 29 where magnitudes represent absolute values, this is reason why they are positive. It can be seen from Figure 28 that F_8 is equal to zero (connection problems), F_3 and F_6 are very small but not zero. There were connection problems with a sensor mounted on the pusher plate number four in tests series 1, 2 and 3; therefore it is left out, see Figure 29.

$$Q_{12} = (F_1 + F_2)/2{,}5 \text{ m} \quad \textbf{(9)}$$

$$Q_{34} = (F_3 + F_4)/2{,}5 \text{ m} \quad \textbf{(10)}$$

$$Q_{56} = (F_5 + F_6)/2{,}5 \text{ m} \quad \textbf{(11)}$$

$$Q_{78} = (F_7 + F_8)/2{,}5 \text{ m} \quad \textbf{(12)}$$

$$Q_{14} = (F_1 + F_2 + F_3 + F_4)/5 \text{ m} \quad \textbf{(13)}$$

$$Q_{36} = (F_3 + F_4 + F_5 + F_6)/5 \text{ m} \quad \textbf{(14)}$$

$$Q_{58} = (F_5 + F_6 + F_7 + F_8)/5 \text{ m} \quad \textbf{(15)}$$

$$Q_{16} = (F_1 + F_2 + F_3 + F_4 + F_5 + F_6)/7{,}5 \text{ m} \quad \textbf{(16)}$$

$$Q_{38} = (F_3 + F_4 + F_5 + F_6 + F_7 + F_8)/7{,}5 \text{ m} \quad \textbf{(17)}$$

$$Q_{18} = (F_1 + F_2 + F_3 + F_4 + F_5 + F_6 + F_7 + F_8)/10 \text{ m} \quad \textbf{(18)}$$

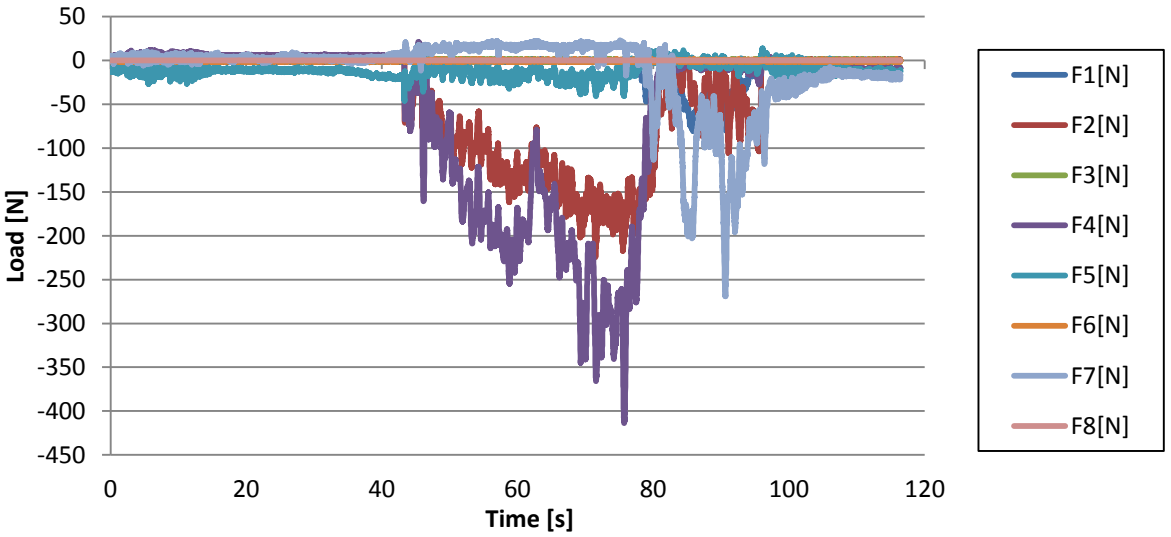

Figure 28 *Time histories measured at the pusher plates during the sixth test run in the second test series.*

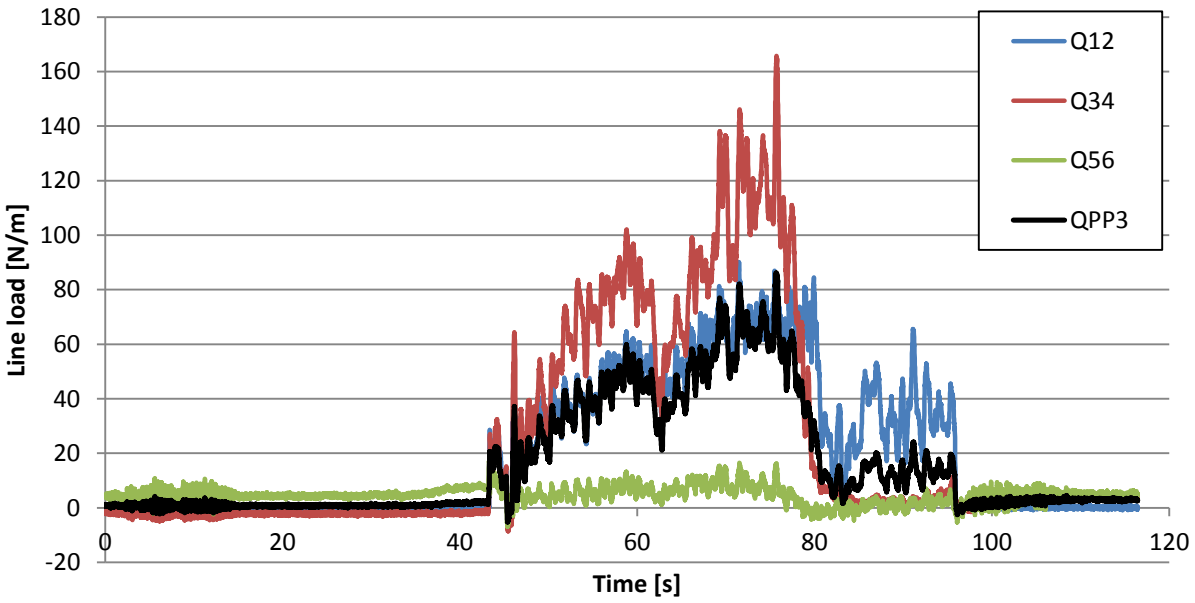

Figure 29 *Time histories calculated line loads for each pusher plate and sum of line load acting on three pusher plates during the sixth test run in the second test series.*

Because of better interpretation, only the highest value of line loads which acting on pusher plates will be presented with one value for different width. The highest line load acting on one pusher plate, Q_{PP1}, is derived comparing maximum line loads of Q_{12}, Q_{34}, Q_{56} and Q_{78}. For two adjacent pusher plates, Q_{PP2} is obtained comparing maximum line loads from Q_{14} to Q_{58}. Q_{PP3} represents the highest line loads acting on three pusher plates in sequence and it is obtained comparing maximum of Q_{16} and Q_{38}. Q_{PP4} is equal to maximum of Q_{18} and represents

line load acting on four pusher plates. For example, in the test 2_6 (Figure 29), the highest line load for one pusher plate is equal to maximum of Q_{34}, apropos Q_{PP1} = 165.8 N/m, while the highest line load for three pusher plate is Q_{PP3} = 86.2 N/m. The highest values of line loads for each line load width are displayed in tables in APPENDIX.

As mentioned above, midship load panel was equipped with three one-axial sensors, sum of those three forces give total force acting on midship load panel, see Figure 30. Line load along the midship load panel is calculated using equation (19):

$$Q_{midship} = (F'_1 + F'_2 + F'_3)/l_{midship} \quad \textbf{(19)}$$

where F'_1, F'_2 and F'_3 are measured forces at midship, $l_{midship}$ is 0,3 meters, length of the load panel at the midship.

Forces measured on load panel at the bow shoulder show that forces in X and Y directions can be neglected (Figure 31). Total force on bow shoulder is equal to F_z, and line load at bow shoulder is

$$Q_{bowshoulder} = F_z/l_{bowshoulder} \quad \textbf{(20)}$$

where $l_{bowshoulder}$ is 0,12 meters, length of the load panel at the bow shoulder.

Although, from these two figures may seem that the loads are higher at midship, measured force truly is bigger, but because it acts over the wider area, usually line loads are equal to or less than those which acting on bow shoulder. This can be observed from the figures and date presented below in work. Also, as it is case with pusher plates, only maximum load at the bow shoulder and midship will be considered. For instance, the highest line load in the sixth test run in the second test series, $Q_{midship}$= 824.2 N/m, is obtain dividing maximal force acting on load panel at midship, 247.3 N (Figure 30), with width of load panel, 0.3 m.

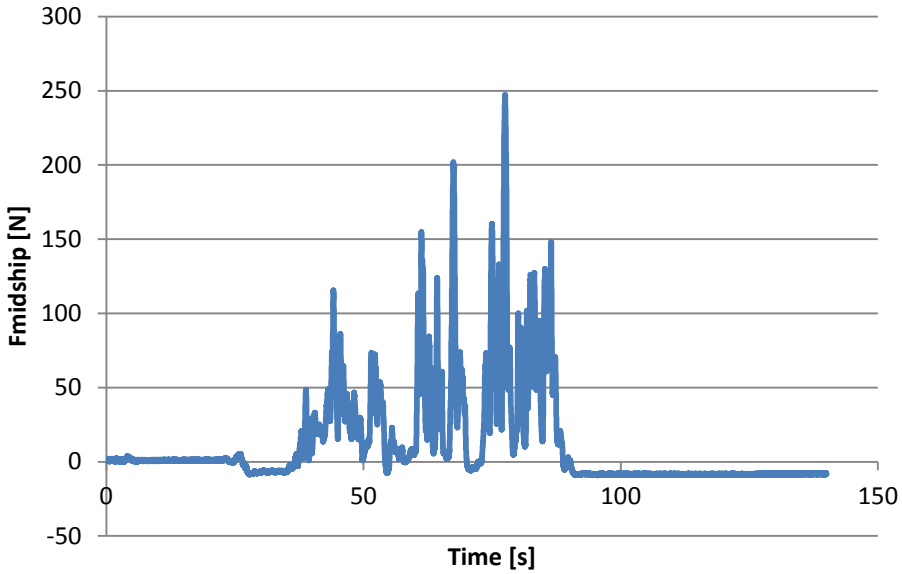

Figure 30 *Time histories total force on midship load panel during test 2_6.*

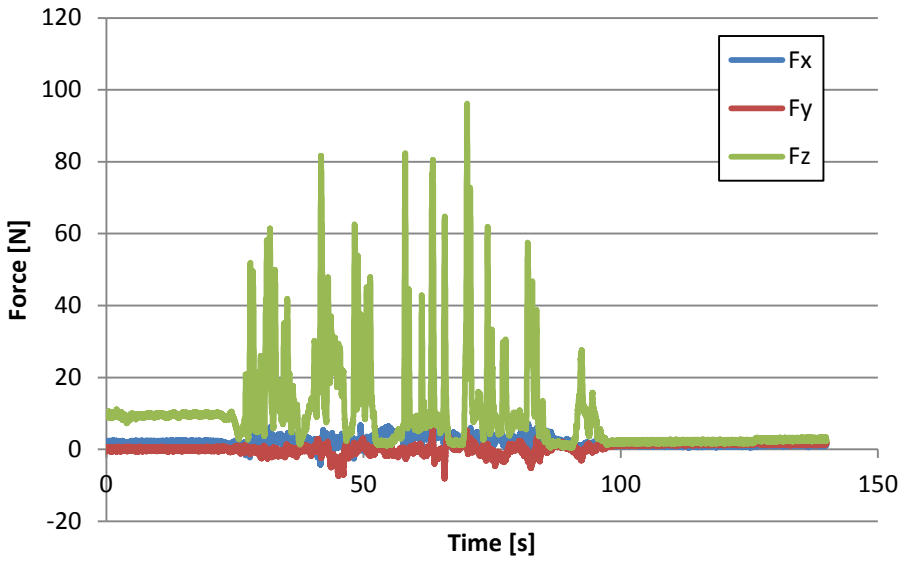

Figure 31 *Time histories total force on bow shoulder load panel during test 2_6.*

5.2. Compression level ice test

The compression in compressive level ice tests is considered to be static compression as compression existed in the ice sheet and the speed of the sheet was close to zero. As the bridge was adjusted to move 0.002 m/s, except test 4_2 where the speed is unintentionally set-up 0.02 m/s, the channel behind the ship model did not closed and the intact ice sheet carried the load inserted by the pushing plates. Furthermore, the highest value of line loads for each line load width is obtained on the same way as in section 5.1. Figure 32 shows channel after compressive level test 3_2. It can be seen that the channel is completely open. Also in the middle of the basin level ice is broken from channel to pusher plates.

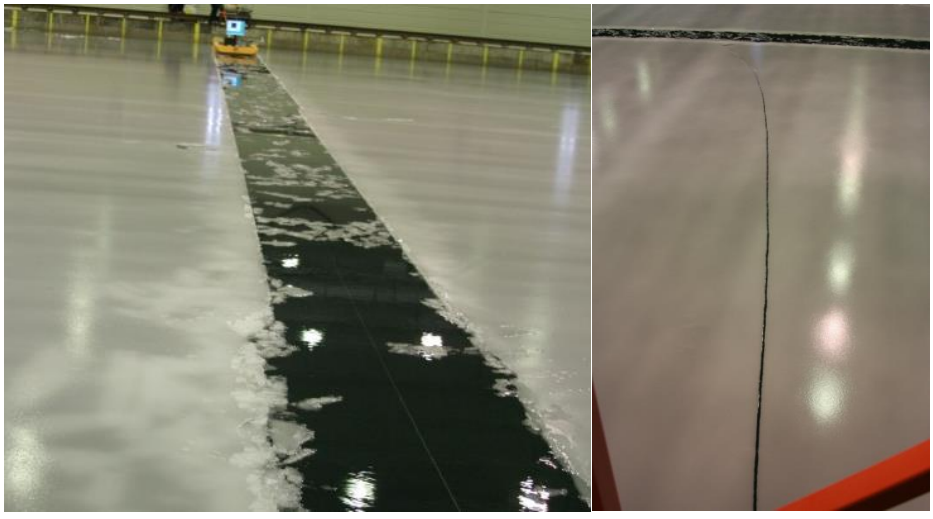

Figure 32 *Channel after compressive level ice test 3_2 (left) and fracture in the ice (right). The channel was close to straight line and the cusps were very small.*

As can be observed from Figure 33, tests 1_2 and 4_2 have highest line loads. This is because thicker ice was used in test 1_2, while in test 4_2 the ice speed was higher. Moreover, test 3_2 has the lowest values because of thinner ice. Measurements at midship load panel show that

compression wasn´t happened in test 6_2 and week compression was occurred in test 3_2 and test 5_2. Reason why measured loads in tests 6_2, 3_2 and 5_2 are significantly smaller might be broken ice sheet, see Figure 32. Measurements show a large scatter of values for the local area because of the stochastic nature of the ice. This and thicker ice are reasons way measurement at bow shoulder in test 1_2 is much higher than other tests.

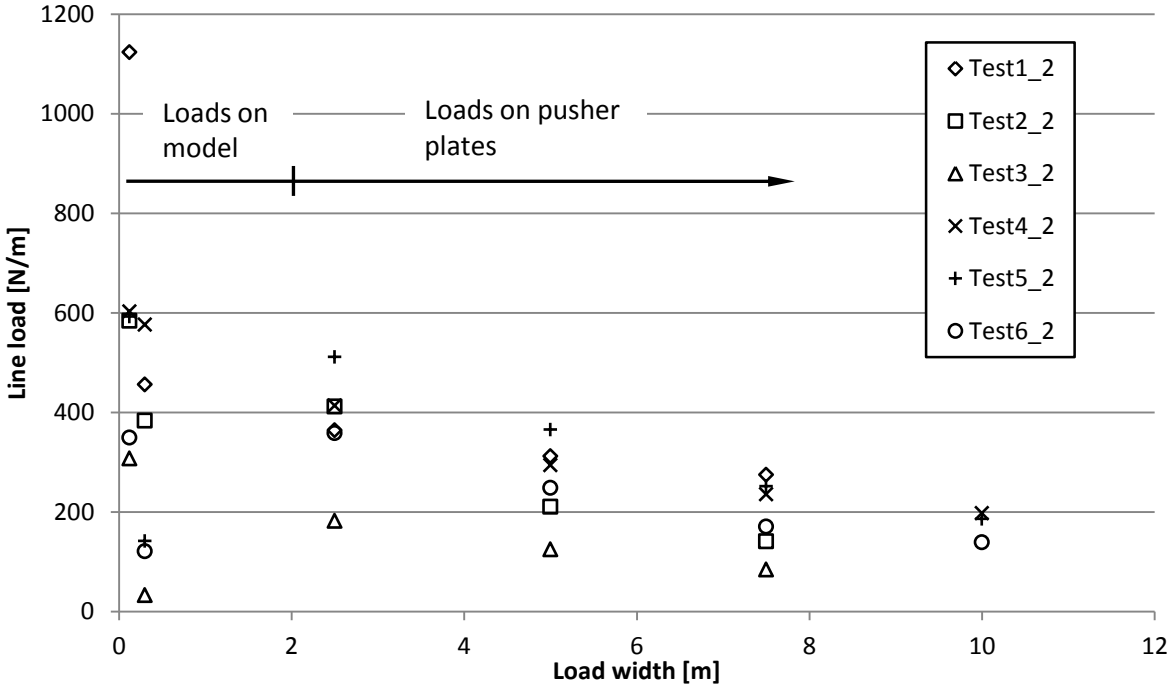

Figure 33 *The maximum line loads for different width in compressive level ice tests.*

5.3. Closing channel test

Compression in closing channel is considered to be dynamic compression. There were conducted 28 closing channel tests. For every test, the highest value of line loads for each line load width is obtained as it is in section 5.1. In the testing one of the main goals was to achieve different compressive conditions in closing channel by varying compression level and ice thickness. The channel closed quite quickly with speed of 0.01, 0.02, 0.03 and 0.04 m/s. In tests with higher ice speed channels were closed before and after model during the tests while tests with lower ice speed, channels weren't closed at all. Figure 34 and Figure 35 show picture during test 5_8 and after test 6_3, respectively.

Figure 34 *A picture from closing channel test 5_8 with ice velocity 0.03 m/s. It can be seen that channel was closed after and before model and the ice sheet was broken. Rubble ice is the reason why channel looks like it is closed immediately after model.*

Figure 35 *Picture from closing channel test 6_3 with ice velocity 0.01 m/s.*

Figure 36 and Figure 37 show the highest values of line loads for each line load widths in the fourth and fifth test series. Although these tests have the same ice thickness, because of the different properties of ice, they are presented in two charts. As can be seen, maximum line loads at bow shoulder and midship are almost 1000 N/m and with the increase of width, line loads tend towards 150 N/m. As expected, the values of the line loads in these two test series are approximately the same.

The line loads in the sixth test series (Figure 38) are lower than line loads in the fourth and fifth test series. This is due to thinner ice. Maximum line loads at bow shoulder and midship are around 850 N/m and with increase of width, line loads tend to 100 N/m.

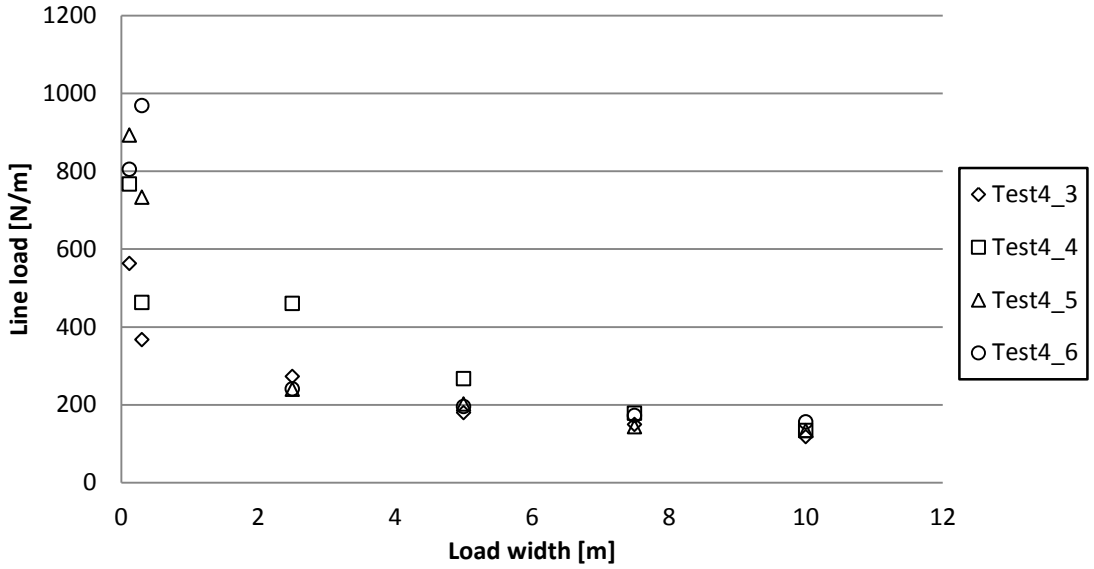

Figure 36 *Line loads at bow shoulder, midship and pusher plates in the fourth test series (ice thickness 29 mm).*

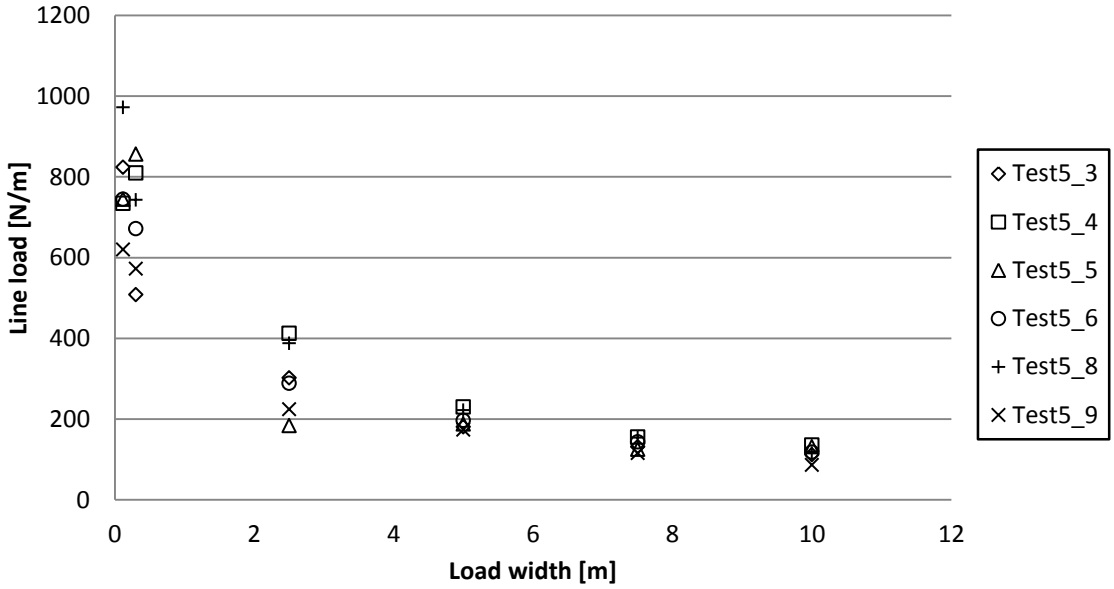

Figure 37 *Line loads at bow shoulder, midship and pusher plates in the fifth test series (ice thickness 29 mm).*

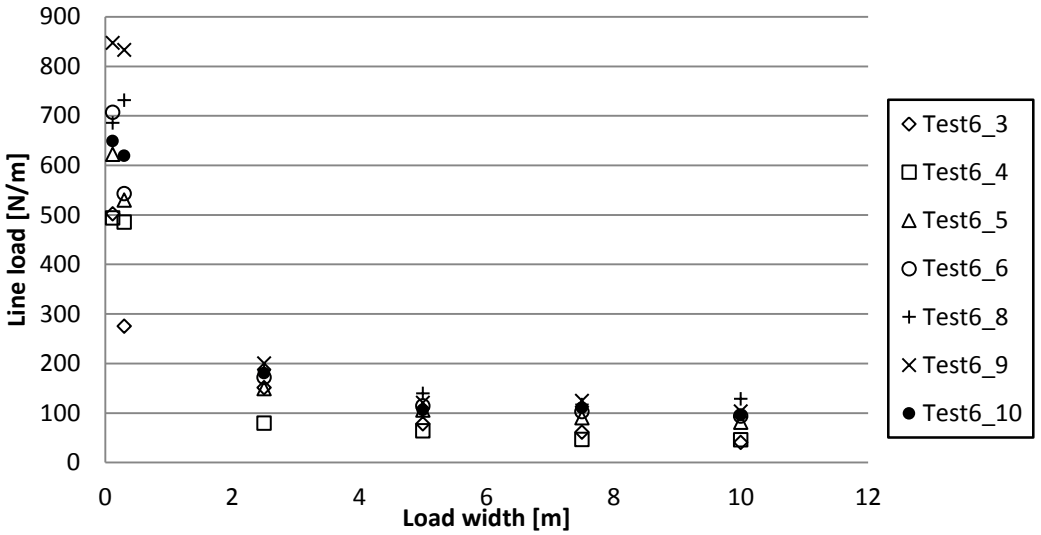

Figure 38 *Line loads at bow shoulder, midship and pusher plates in the sixth test series(ice thickness 24 mm).*

The fourth and fifth test series have the same ice thickness (29 mm), so their line loads in all tests are compared depending on ice velocity, see Figure 39. Figure 40 shows maximum line loads at the pusher plates and model during the sixth test series. The tests having the lower closing speed were conducted before the tests with higher speed. Although, the highest velocity of ice did not cause the highest line loads (in the sixth series all maximum values were with speed less than 0.04 m/s), in general, increasing of ice speed leads to increase in line load. A reason for this can be micro-cracks in the ice formed by tests before, which eventually led to rupture of the ice, see Figure 32.

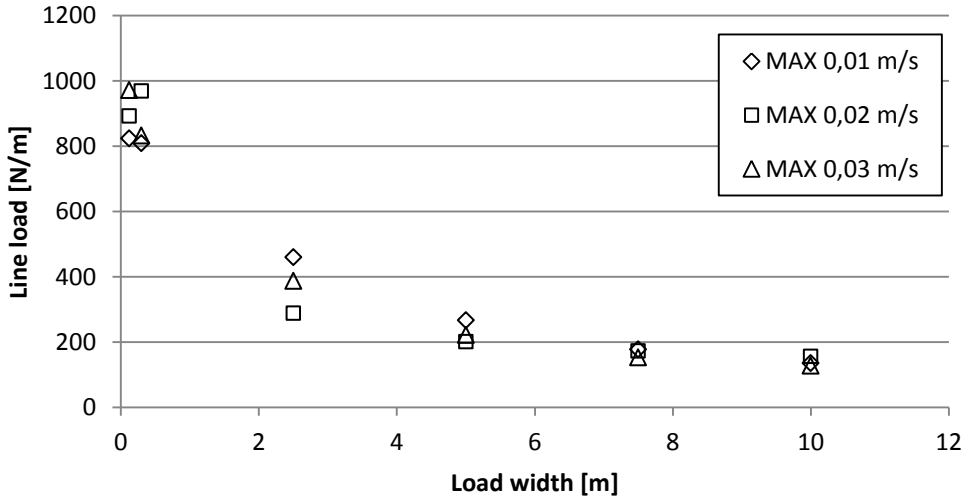

Figure 39 *The maximum line loads for different ice speed measured at pusher plates and model during fourth and fifth test series (ice thickness 29 mm).*

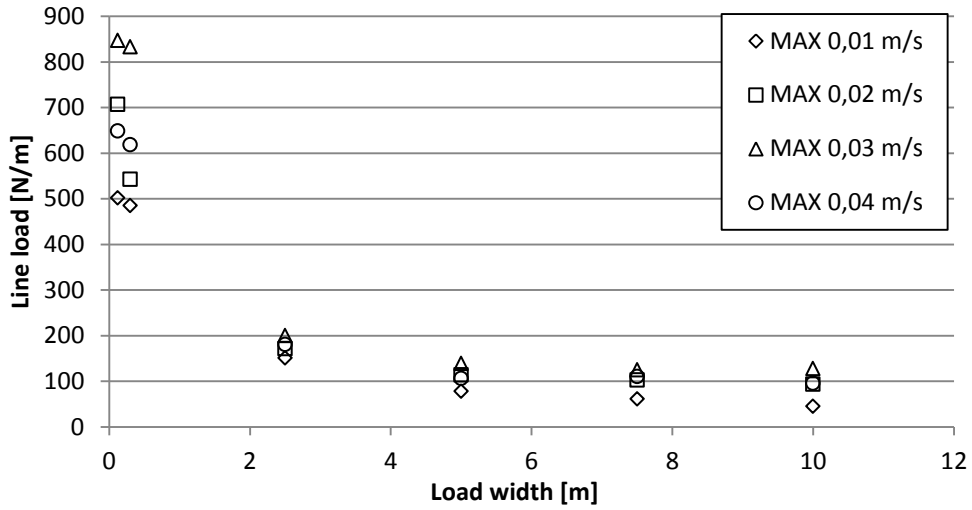

Figure 40 *The maximum line loads for different ice speed measured at pusher plates and model during the sixth test series (ice thickness 24 mm).*

Figure 41 shows the highest values of line loads at the bow shoulder, midship and pusher plates in the third test series. Line loads are similar to line loads from the sixth test series because ice thickness and compressive strength is almost equal in spite of different ice velocity in some tests. An equal ice speed (0.03 m/s) was used for the first, second and third test series. Even though the ice thickness is the same in the second test series (Figure 42) with ice thickness in the fourth and fifth test series (Figure 36 and Figure 37), line loads are a little lower. A less strong ice, compressive strength was only 50.5 kPa, was used in the second test series, this explains why line loads are lower. As can be observed from Figure 43, line loads for the 1st test series are much higher than loads from Figure 41 and Figure 42, as well as from Figure 36, Figure 37 and Figure 38. The maximum line loads at bow shoulder is more than 2300 N/m and at midship is almost 2000 N/m with the increase of width, line load tends towards 300 N/m.

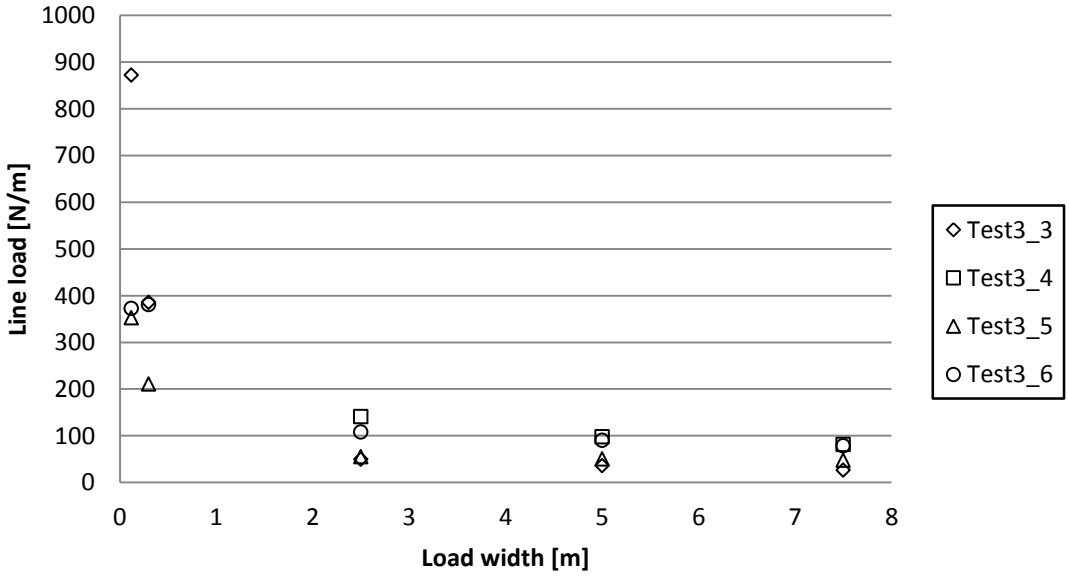

Figure 41 *Line loads at bow shoulder, midship and pusher plates in the third test series (ice thickness 23 mm).*

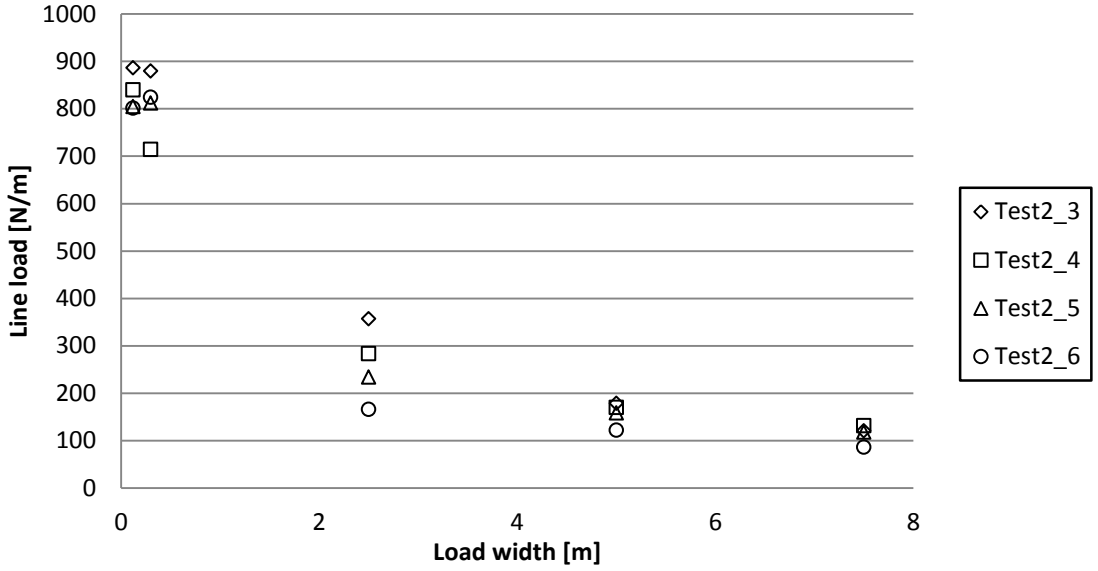

Figure 42 *Line loads at bow shoulder, midship and pusher plates in the second test series (ice thickness 29 mm).*

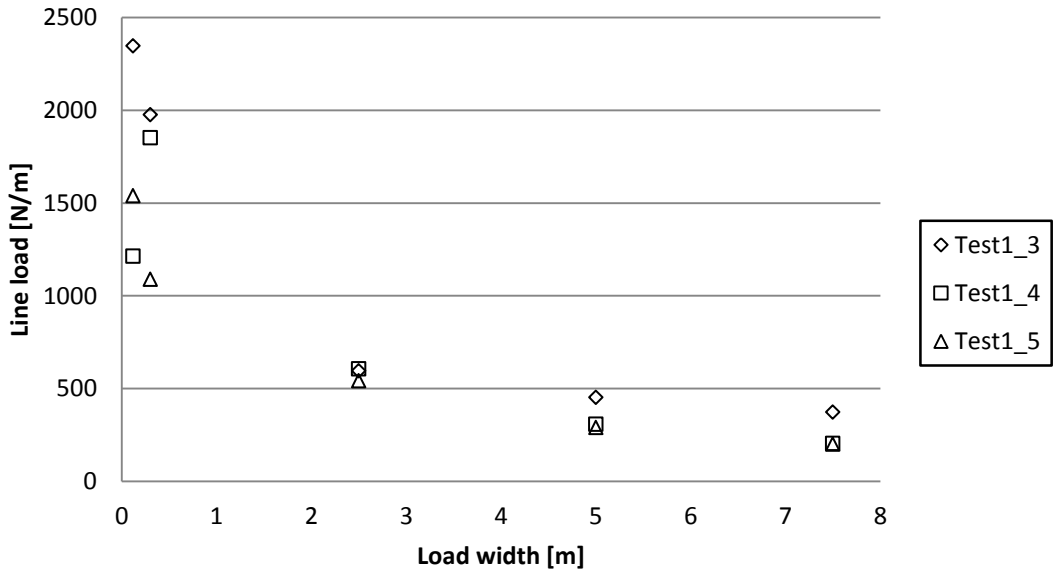

Figure 43 *Line loads at bow shoulder, midship and pusher plates in the first test series (ice thickness 40 mm).*

5.4. Defining line load curve

After analyzing all the tests, the results are presented with the curve line load. The line load curve, line load and load width relationship, is provided for illustrative purposes and for comparison to other model tests, observations or numerical methods. In this case, line load curve is defined with highest loads measured on the model and the pusher plates, because maximum loads are relevant to design ship.

Figure 44 shows line loads at the model and pusher plates from all closing channel tests. Obviously, linear loads are the highest in the first test series, because of the speed and thickness of ice. A large scatter of values was attributed to different ice properties and

compression level, as well as stochastic nature of the ice. Due to the lack of measured force at the pusher plate 4 (F_8) caused by the connection problems in the first three test series, line loads at four pusher plates was compared in other three test series and the maximum load line is Q_{18} =155.88 N/m in test 4_6.

Figure 45 presents the maximum line load for a different ice thicknesses measured at the bow shoulder, midship and pusher plates as a function of loading width. Curves were fitted to the data points of the bow shoulder, midship and pusher plates, see the fitted line in Figure 45, using the least mean square fit. The equation (21) for the curve was of the form

$$q = C\left(\frac{l_c}{s}\right)^{-a} \quad \textbf{(21)}$$

where q is line load, C and a are unknown parameters, l_c is the contact length and s is the smallest load width obtained by scaling the typical full scale values of frame spacing to model scale. In a full scale, the typical values are around 350 mm [7], which is 0.014 meters in the model scale used in this study. Table 11 presents the parameter values defined for the fitted curves for the bow shoulder and the midship and the coefficient of determinations. As can be observed from Figure 45 and the values of the coefficient of determination, the curves give a good presentation for the data points. Also, because there is no data for the pusher plate 4 in the first test series, the value of the line load for all pusher plates has been taken from the other tests.

Table 11 *The parameter values for the fitted lines and the coefficient of determination.*

	C [N/m]	a	s [m]	R^2
Ice thickness 40 mm (Figure 43)	9182,4	0,546	0,014	0,9259
Ice thickness 29 mm (Figure 36, Figure 37 and Figure 42)	3054,6	0,427	0,014	0,9269
Ice thickness 23 and 24 mm (Figure 41and Figure 38)	2983,1	0,501	0,014	0,9681

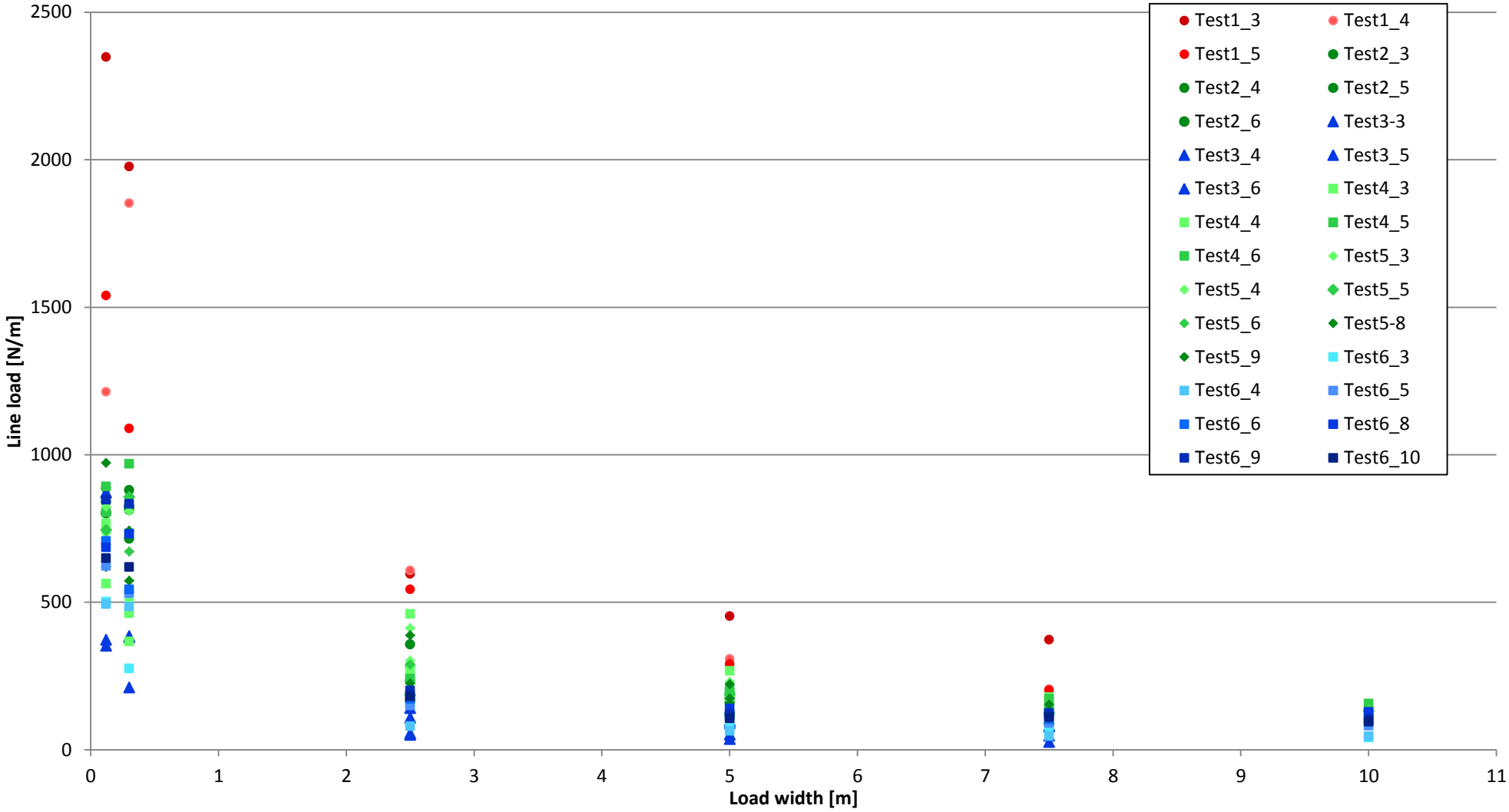

Figure 44 *Line loads at bow shoulder, midship and pusher plates in all test series. Because of the same ice thickness, the 2nd, 4th and 5th test series are marked with one color (green) but with different marker types, as well as the 3th and 6th test series (blue), where ice thicknesses were almost the same. Moreover, tone of lighter color represents a lower ice speed, while darker tone refers to the higher speed.*

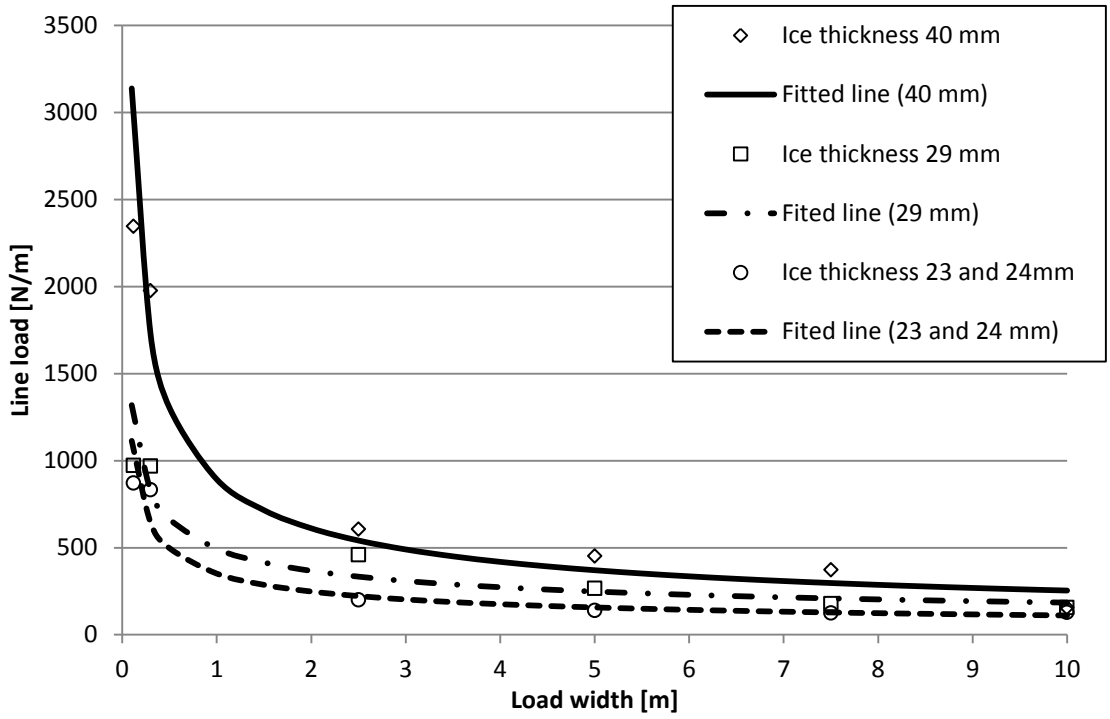

Figure 45 *Maximum line load defined for different ice thicknesses and related line load curves (fitted lines).*

6. ISO CODE

In this chapter two methods for evaluating the average global pressure are described. In general, the ISO recommend different approaches for evaluating ice loads depending on the age of the ice, the slope of the structure, area where load acting, etc. Chapter "A.8.2.4.3.3 Global pressure for sea ice" and "A.8.2.4.3.5 Global ice pressures from ship ramming tests" from ISO 19906 [45]are described, other methods aren't suitable to compare with ice model tests mentioned above or aren´t in the scope of this work.

The series of International Standards ISO 19900 to ISO 19906 addresses design requirements and assessments for all offshore structures used by the petroleum and natural gas industries worldwide. Through their application, the intention is to achieve reliability levels appropriate for manned and unmanned offshore structures, regardless of the type of structure and the nature or combination of the materials used.

6.1. Global pressures from sea ice

Figure 46 shows the structure of an hpz, and the appearance of these within a plane of interaction. Within the hpz's, the state of stress in the ice is tri-axial, varying from low confinement near the edges to high values of contact pressure near the centre.

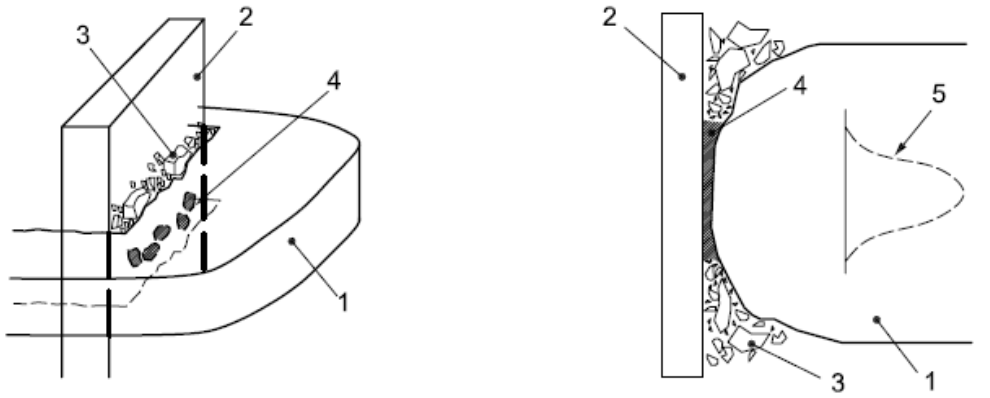

a) Ice sheet interaction with the flat surface of a narrow vertical structure

b) Profile of ice sheet interaction with vertical structure

Key

1 ice sheet
2 structure
3 spalls and extrusion
4 high pressure zones in a), layer of crushed ice of high pressure zone in b)
5 pressure distribution over the contact surface

Figure 46 *Schematic showing localization of action in compressive ice-structure interaction* **[45]**.

Data obtained from full-scale measurements in Cook Inlet, the Beaufort Sea, Baltic Sea and Bohai Sea have been used to determine upper bound ice pressure values for scenarios where a first-year or multi-year ice acts against a vertical structure. The data have also been used to

analyze how the ice thickness and the width of the structure influence the global ice action. Based on these studies, the global ice pressure can be determined as given in equation (22):

$$p_G = C_R \left(\frac{h}{h_1}\right)^n \left(\frac{w}{h}\right)^m \quad \textbf{(22)}$$

where

p_G is the global average ice pressure, expressed in megapascals;
w is the projected width of the structure, expressed in meters;
h is the thickness of the ice sheet, expressed in meters;
h_1 is a reference thickness of 1 m;
m is an empirical coefficient equal to −0,16;
n is an empirical coefficient, equal to $-0.50 + h/5$ for $h < 1.0$ m, and to −0.30 for $h \geq 1.0$ m;
C_R is the ice strength coefficient, expressed in megapascals.

Equation (22) applies for rigid structures with aspect ratios w/h greater than 2. Further, in a deterministic analysis, the strength parameter for ELIE can be assumed as $C_R = 2.8$, based on first-year and multi-year data from the Beaufort Sea. This C_R value can be conservative as it potentially includes some magnification due to the compliance of the structure in the referenced data from the Beaufort Sea.

According to another data series from a stiff structure in the Baltic Sea, the ELIE ice strength parameter has been obtained as $C_R = 1.8$ in conditions where the ice speed was higher than 0,1 m/s and the maximum waterline displacements in the direction of ice action of the structure were about 0,4 % of the ice thickness. Under these conditions, the strength value C_R obtained does not exhibit magnification due to the compliance of the structure. The same data set indicates that C_R is about 15 % to 20 % higher for ALIE, so ELIE generally governs level ice actions on vertical structures.

6.2. Global ice pressures from ship ramming tests

Data from ship rams into multi-year ice indicate that the global action is random, even for seemingly identical rams. This is associated with random fracture events in the ice as it fails. Because of size effects, the average global pressure generally decreases as a function of nominal contact area. The pressure-area relationship as given by equation (23) has been developed for impact scenarios:

$$p_G = C_P {A_N}^{D_P} \quad \textbf{(23)}$$

where

A_N is the nominal contact area, it is product of the ice thickness, h, and the width, w;

C_P and D_P are random coefficients.

The coefficients C_P and D_P have been calibrated using a large database of ship rams with multi-year ice (Kigoriak, Polar Sea, MV Arctic, Manhattan and Oden). The projection of the

original shape of the ice feature onto the structure at the appropriate penetration and the resulting maximum actions for each simulation were then ranked and compared on a probability of exceedance basis with ship ram trial data. A goodness-of-fit criterion was used to decide which combination best represented the coefficients. The preferred combination was a mean and standard deviation of 3.0 and 1.5, respectively, for C_P (lognormal distribution) and a mean and standard deviation of −0.4 MPs and 0.2 respectively, for D_P(normal distribution).

6.3. Modification ISO code from global ice pressure to line load

For a purpose of this work, loads given by ISO in equations (22) and (23) are modified from pressure to line load to be comparable with results from previous chapter, see equation (24). Below in the text, chart and tables with values of mean and standard deviation of coefficients for ship ramming test, and parameters for load from sea ice are given.

When ice crushing occurs against a structure, the ice action to the load width, Q, can be expressed as given:

$$Q = p_G h \tag{24}$$

where

Q is the line load, expressed in Newton per meters;

h is ice thickness, expressed in meters.

In Table 12 are displayed parameters for load from sea ice. Line load from sea ice, as well as curves of a mean and standard deviation for ship ramming test are presented from comparison purpose in Figure 47. Loads defined by a mean plus standard deviation are much higher than other line loads; this can be due to coefficients C_P and D_P have been calibrated using a large database of ship rams with multi-year ice. Also, the line loads is decreasing as a function of width. The line load curves of a mean and standard deviation are determined with equation (24) applying the parameter values presented in Table 13.

Table 12 *The parameter values for curves load from sea ice.*

C_R [MPa]	h [m]	h_1 [m]	m -	n -
1.8	0.725	1	-0.16	-0.355

Table 13 *The parameter values for the curve for ship ramming test.*

	C_P	D_P	h [m]
Mean value	3	-0.4	0.725
Mean + Standard deviation	4.5	-0.2	0.725
Mean - Standard deviation	1.5	-0.6	0.725

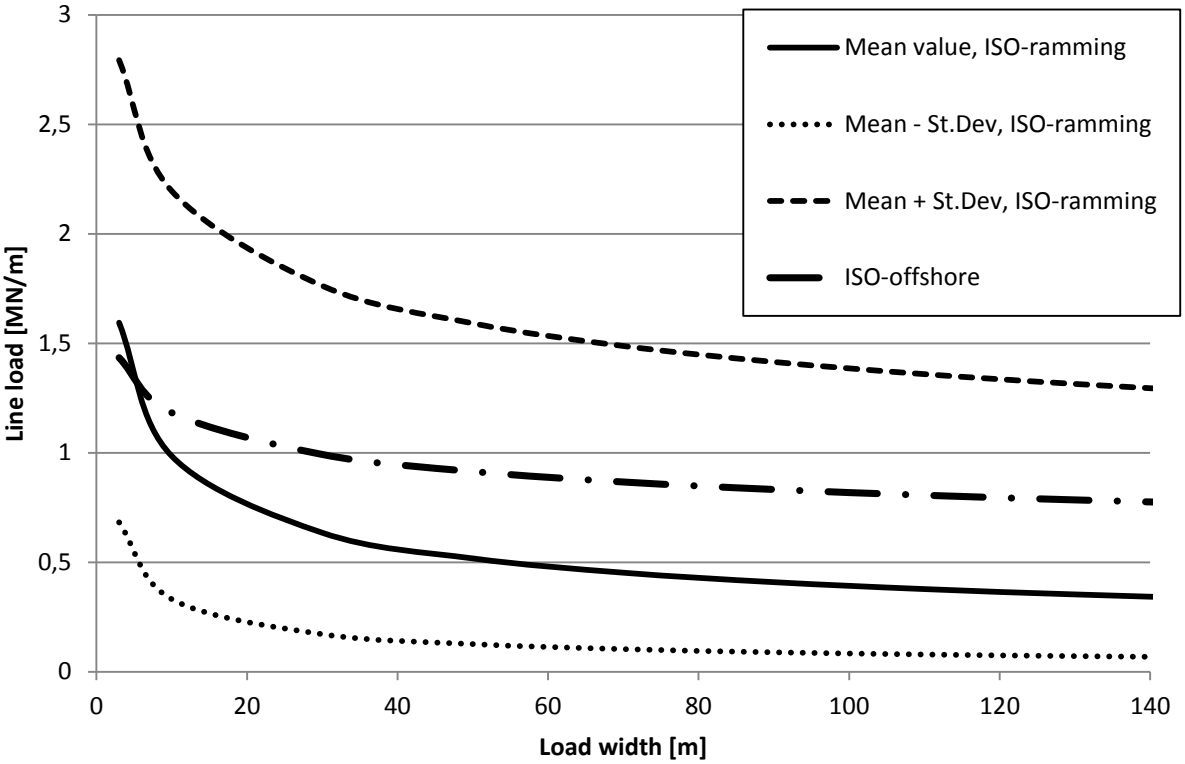

Figure 47 *The line load and load width relationship for a mean and standard deviation as given by equation* (**24**).

7. COMPARISON BETWEEN ISO, MODEL SCALE TEST RESULTS AND SOME FULL SCALE MEASUREMENTS

In order to check the dependability of data obtained from ISO code in previous chapter, the line loads have to be compared with results of model test in Chapter 5. Moreover, results are compared with full-scale measurements on ships. As the compressive situation is not widely studied, the amount of data available is limited. Nevertheless, the results of the model test are compared with two different data sets in this chapter.

As mentioned above, tests were conducted in level ice and in channel. Line load curves are defined as a function of load widths for closing channel tests, so these curves are compared. To allow for comparison with full-scale field data, the line load data from the model-scale tests were scaled to full-scale by multiplying it by λ^2, the load width and ice thicknesses are converted to full scale by multiplying it by λ.

7.1. Full-scale comparison of test result and ISO code

Calculated line loads from previous chapter are compared with line loads from model tests, see Figure 48. As can be seen, all three fitted lines for different ice thicknesses are between the mean and mean minus standard deviation recommended by ISO code. Obviously, the maximum value (mean plus st.dev.) is too exaggerated for these tests due to database for multi-year ice which is, predominantly, more compact e.g. stronger than the first-season ice. Other reason can be that database consist loads in ridge fields, which cause higher measured loads. However, results from two methods, model testing and Global ice pressure from ship ramming tests, are comparable. Further, load from sea ice on offshore structure doesn't describe well line loads from tests. This can be because ISO recommend this method for a rigid structure.

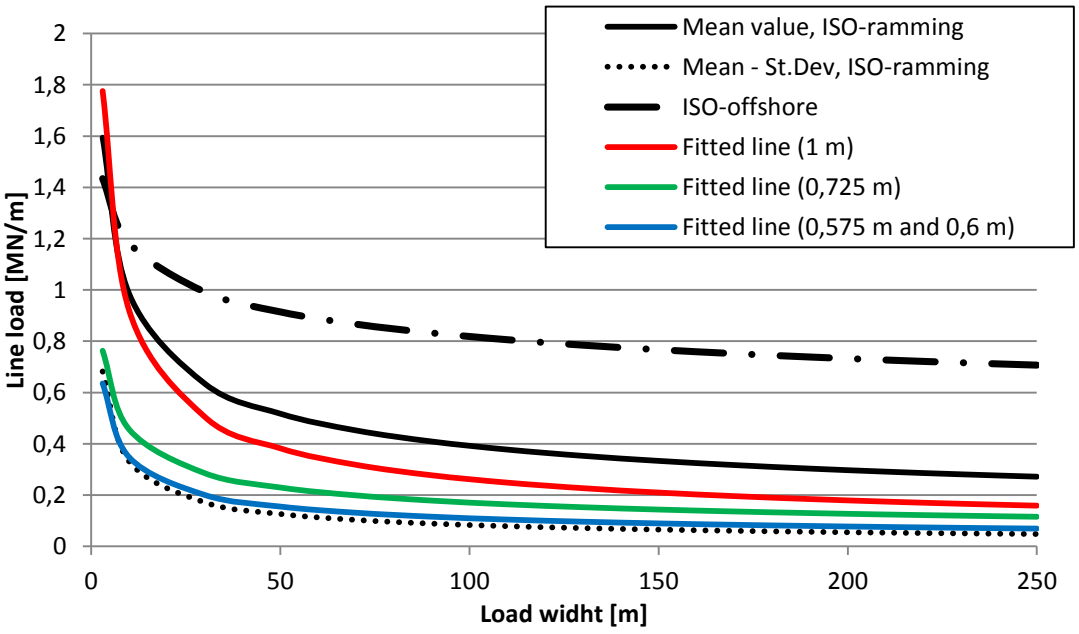

Figure 48 Model scale data scaled to full scale. Comparison of ISO code and the maximum line loads for different ice thicknesses.

7.2. Full-scale comparison of test result with IB Sisu and MS Arcturus

As mentioned above, measurements from IB Sisu and MS Arcturus are in the ship scale. Line loads from model testing are higher than line loads from MS Arcturus, see Figure 49. Moreover, difference is insignificant for line loads from model test for 0.575 m and 0.6 m thick ice (the 3th and 6th test series) and IB Sisu. Also, comparing line loads measured on IB Sisu and those from the 2nd, 4th and 5th test series (0.725 m thick ice), line loads in testing are slightly higher. The difference is more significant in narrower load widths, but the line loads measured in tests are approaching the line loads measured on the IB Issus in greater load widths. Although, the maximum ice thickness varied from 1.07 to 1.10 m with a higher probability of ice ridges or rafts, line loads in the 1st test series (Fitted line 1 m) are higher than those from IB Sisu. This can be because data from IB Sisu are gathered at the bow where slope is smaller comparing to the bow shoulder in model testing, where hull shape (load panel) is almost perpendicular with ice, causing larger force than those on bow where ice bending failure occurred much easier, i.e. lower force is needed to break the ice.

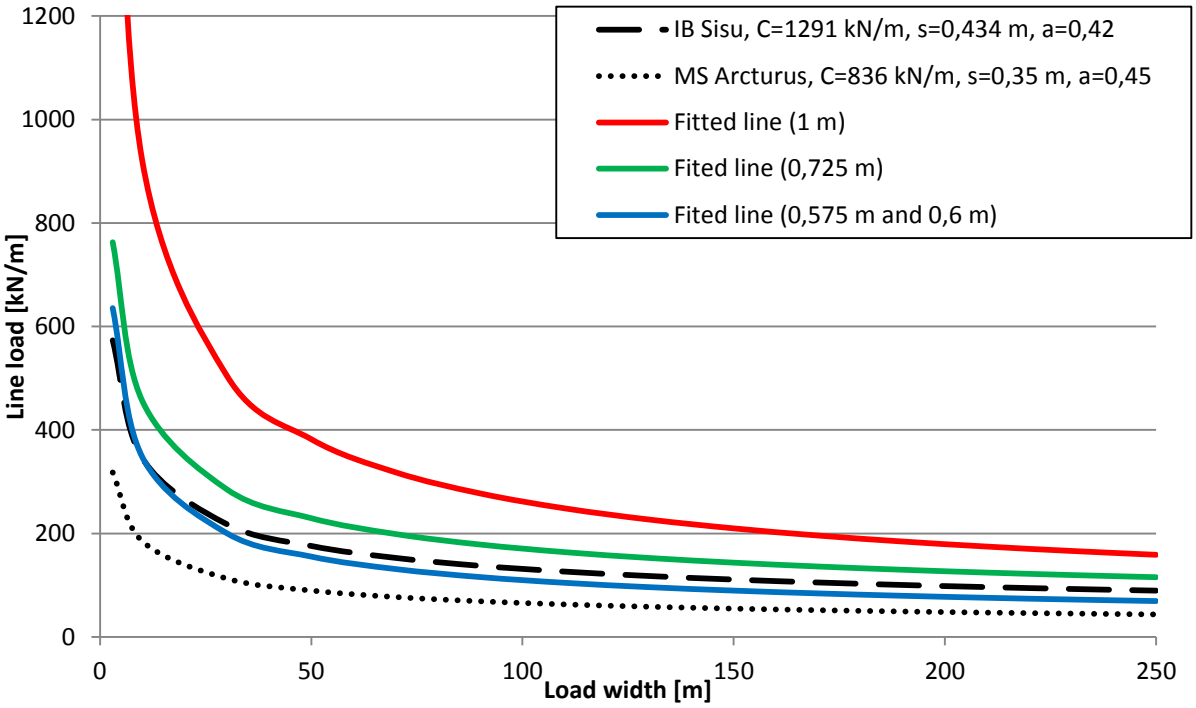

Figure 49 *Model scale data scaled to full scale. Comparison with IB Sisu and MS Arcturus full scale measurements.*

8. DISCUSSON

Compressive level ice tests were conducted once for every test series. Measurements show a big scatter of values for the local area. In spite of the fact that ice speed was the same for all tests, except test 4_2 where speed was 0.02 m/s, measurements at the midship show that different compression levels were occurred. Reason for that might be that thin ice, in this case tests 3_2 and 6_2, was fractured from channel to the pusher plate during the tests, so measured loads at the midship were very weak.

Alltogether 28 closing channel tests were conducted where the ice thickness and compression level were varied. Generally, increasing of ice speed (load compression) leads to increase in line load. Results show that case with the highest compression (ice speed) does not give the maximum loads on model. One possible reason for this is that after a certain point the ice sheet fails, or reaches the ultimate strength, after which the ice is severely compromised. This would explain the decrease of load due to compression. Moreover, comparing level ice and closing channel measurements, loads at the bow shoulder and midship were higher in closing channel tests, however, they are slightly higher on the pusher plates in compressive level ice test. Obviously, loads from pusher plates were transmitted through ice sheet in front of model and on the model hull. In closing channel tests, loads from pusher plates were distributed only on the model's hull causing higher loads on the model.

Comparison of ISO code for ship ramming tests and results from model testing give good correlation. Line loads for different ice thicknesses from model testing are lower than the mean value recommended by ISO. This is more reasonable than the case where line loads will be higher than mean value because loads from ship ramming test have been calibrated using a database of ship rams with multi-year ice. Further, line loads from tests are higher than the minimum value, this means that they are within recommended area. In addition, load form sea ice on offshore structure is too exaggerated. Increasing the width, difference between load from sea ice on offshore structure by ISO and test results is bigger which causes that the load from sea ice is 4-6 times higher than line loads from pusher plates.

In the second comparison, ice model test results are compared with full-scale data measured at bow area on IB Sisu and MS Arcturus. Obviously line loads from model tests are higher than measured on ships. One of the reasons for this difference is because measurements on IB Sisu and MS Arcturus were conducted at the bow area while in model tests at the bow shoulder and midship area. Furthermore, considering that model had a high block coefficient and a long parallel midship section, it can be claimed that applied model hull is less suitable for ice conditions than IB Sisu. This assumption can be for MS Arcturus too, because she is smaller than Credo which means shorter parallel midship section, and also she doesn't have high block coefficient while Credo has. Another reason why measured loads on MS Arcturus are lower is that the main navigation area in ice is the Gulf of Finland, where ice is thinner than 1 meter. Moreover, the channel broken by the model was close to straight line and the cusps were small. This means that dominant ice failure mode was crushing, at least at the midship area. This causes that the distance between hull and ice edge is small and hull-ice interaction

continues soon after the bow shoulders that result in higher loads at the midship area. The hull shape is not parallel to the ice sheet at the bow shoulder which enables the ice to break through bending and shear failure. This explains why line loads at the bow shoulder and midship were similar in some cases because if the ice breaks through bending or shear failure, the measured loadings are smaller than when it would have broken through crushing.

9. CONCLUSIONS

The focus of this work was on the line load at ship hull in compressive level ice and closing channel tests. The effect of the ice thickness and the compression level on the ice loads on the model hull is studied. Measured loads are analyzed and presented. The measurements from the load panel at the bow shoulder, midship and at the pusher plates in model scale give realistic distributions for the ice induced loads in level ice conditions for various types of compression and ice thicknesses.

The analyzed results show that ice thickness has a major influence on the loads. Also, compression level has influence on loads, but significantly less than thickness. Increasing ice thickness, the ice piles obtained by hull-ice interaction are bigger. Furthermore, fracturing of ice sheet can have a big influence on the measurements. When rupture occurred, decrease of load was recorded.

The fitted curves give good presentation from the data points and are comparable to the other data. Value of the line load is smaller with greater load width. The contact line showed that the average line load is higher if the load width decrease. Significant increase of line load was occurred when the contact width decrease less than 0.5 meters in model-scale. In addition, based on the results of tests, the line load due to compression was compared with ISO methods: global ice pressures from sea ice and global ice pressures from ship ramming tests. The calculated values represented the results of model tests fairly well. Further, global ice pressures from sea ice recommended by ISO can't be used for evaluating ice loads on ships. This method is too conservative and it should be further analyzed for rigid structure.

BIBLIOGRAPHY

[1] Kujala, P., Goldstein, R., Osipenko, N. & Danilenko, V., "A Ship in Compressive Ice, Preliminary Model Test Results and Analysis of the Process, Report from the joint Finnish-Soviet research project," Otaniemi, M-111, 1991.

[2] Riska K., Kujala P., Goldstein R., Danilenko V. & Osipenko N., "Application of Results from the Research Project "A Ship in Compressive Ice" to Ship Operability," in *The 13th International Conference on Port and Ocean Engineering under Arctic Conditions (POAC)*, Murmansk, Russia, 1995.

[3] Leppäranta, Matti, *The Drift of Sea Ice*. Chichester: Praxis Publishing Ltd, 2005.

[4] Eriksson P., Halapa J., Heiler, I., Leisiti H., Riska K. & Vainio J., "Ships in Compressive Ice: Description and Operative Forecasting of Compression in an Ice Field," in *Winter Navigation Research Board, Research Report No. 59*, 2009, p. 42.

[5] Kaups, Kristijan, "Modeling of the ship resistance in compressive ice, Master's Thesis," Aalto University, Depatrment of Applied Mechnanic, Espoo, Master's Thesis 2011.

[6] Leisti, Hanna & Riska, Kaj, "Description of the Compression," , 2010, p. 51.

[7] Kujala, P. & Arughadhoss, S., "Statistical analysis of ice crushing pressures on a ship's hull during hull-ice interaction," in *Cold Regions Science and Technology 70*, 2012, p. 11.

[8] Suominen, M. & Montewka, J., "Model Testing Results WP4 for SAFEWIN," Aalto University (internal report), Espoo, Finland, 2012.

[9] Suominen, M. & Kujala P., "A STUDY OF MEASURED LINE LOAD LENGTHS AND MAXIMUM ICE LOADS ON MODEL SHIP HULL, Aalto University," in *Proceedings of the 22nd International Conference on Port and Ocean Engineering under Arctic Conditions*, Espoo, Finland, 2013, p. 15.

[10] Külaots, Reino, "Numerical and Experimental Modelling of Ship Resistance in Compressive Ice Channels, Master's Thesis," Aalto University, Depatrment of Applied Mechnanic, Espoo, 2012.

[11] Heinonen, Jaako, *Constitutive Modeling of Ice Rubble in First-Year Ridge Keel*. Espoo, 2004.

[12] Ice Atlas, *Climatological ice atlas for the Baltic Sea, Kattegat, Skagerrak and Lake Vänern (1963-1979)*. Norrköping, Finland: Swedish Meteorological and Hydrological Institute & Institut of Maritime Research, 1982.

[13] Kujala, P., Valkonen, J. & Suominen, M., "Maximum Ice-Induced Loads on Ships in the Baltic Sea," , 2007, p. 9.

[14] (2014, February) The Baltic Sea portal. [Online]. http://www.itameriportaali.fi/en/tietoa/jaa/jaatalvi/en_GB/jaatalvi/

[15] Kujala, P., Suominen, M. & Jalonen R., "INCREASING THE SAFETY OF ICEBOUND SHIPPING, FINAL SCIENTIFIC REPORT: VOLUME 1," Helsinki University of Tehnology, Espoo, M-302, 2007.

[16] Kujala P., "On the Statistics of Ice Loads on Ship Hull in the Baltic," Helsinki University of Tehnology, Espoo, MECHANICAL ENGINEERING No. 116 Me 116, 1994.

[17] Swedish Meteorological and Hydrological Institute. (2013, 26.03.) [Online]. http://www.smhi.se/en

[18] Finnish Meteorological Institute. (2013, 15.03.) FMI Polar View Products. [Online]. haavi.fimr.fi/polarview

[19] Joffre, S.M., "Momentum and heat transfers in the surface layer over a frozen sea. Boundary Layer Meteorology 24," 1982.

[20] Cammaert, A.B. & Muggeridge, D.B., "Ice Interaction with Offshore Structures," New York, 1988.

[21] Vaudrey, K.D., "Characterization of Offshore and Coastal Conditions. ASCE Stat-of-the-Practice Report," New York, 1983.

[22] Tuhkuri, J., Lensu, M. & Hopkins, M., "Local Ice Cover Deformations – Laboratory Experiments, Discrete Element Simulations, and Field Observations, Local Ice Cover Deformation and Mesoscale Ice Dynamics," Part 1: Final Scientific Report 1999.

[23] Timco, G.W. & Burden. R.P., "An analysis of the shapes of sea ice ridges. Cold Regions Science and Tehnology," Cold Regions Science and Tehnology, Vol. 25, 1997.

[24] Kankaanpää, P., "Distribution, morphology and distribution of sea ice pressure ridges in the Baltic Sea," Department of Geography, University of Helsinki, Fennia,Helsinki, Doctoral Thesis, 1998.

[25] Høyland, K.V., "The consolidation of first-year sea ice ridges," Vol. 108, No 12, 2002.

[26] Riska K., Kujala P., Goldstein R., Danilenko V. & Osipenko N., "Application of Results from the Research Project “A Ship in Compressive Ice” to Ship Operability," Helsinki University of Technology, Ship Laboratory, 1996.

[27] Sanderson, T.J.O., *Ice Mechanics: Risks to offshore structures*. Boston: Graham & Trotman, 1988.

[28] Delay, C., "Ice Edge Contact: A Brittle Failure Process Model, Acta Polytecnica Scandinavica, Mechanical Engineering Series No.100," , Helsinki, 1991, p. 92.

[29] Delay, C., "A Study of the Process-Spatial Link in Ice Pressure-Area Relationships, PERD/CHC

Report 7-108," , 2004, p. 58.

[30] Kujala P., Goldstein R., Osipenko N. & Danilenko V., "A Ship in Compressive Ice, Analysis of the Ice Failure Process, Report from the joint Finnish-Russian research Project," , 1993, p. 69.

[31] Kendrick, A., "Definition of Ice Loads under the Pressured Ice Scenario, Draft Final Report, Transport Canada," , 1997.

[32] Riska, K. (2008) Forecasting ice pressure against ships. [Online]. http://www.ils.fi/Ice_Day_2008_RISKA.pdf

[33] Varsta, P., "On the mechanic of ice load on ships in level ice in the Baltic Sea," in *Technical Research Center of Finland Publication 11*, Espoo, 1983, p. 91.

[34] Kujala, P., "Semi-empirical Evaluation of Long Term Ice Loads on a Ship Hull," , 1995, p. 23.

[35] Klanac, A., Duletić, T., Erceg, S., Ehlers, S., Goerlandt, F. & Frank, D., "Environmental Risk of Collision for Enclosed Seas: Gulf of Finland, Adriatic, and Implications for Tanker Design," in *5th International Conference on Collision and Grounding of Ships*, 2010, pp. 55-65.

[36] Hänninen, S., "INCIDENTS AND ACCIDENTS IN WINTER NAVIGATION IN THE BALSTIC SEA, WINTER 2002-2003, Research Report No 54," , 2005, p. 44.

[37] Kujala, P., "Damage Statistics of Ice-Strengthened Ships in the Baltic Sea 1984-1987. Winter Navigation Research Board, Research Report No 50," , Espoo, 1991, p. 66.

[38] Juva, M., "An Analysis of Safety of Winter Navigation in the Gulf of Finland Using the FSA-method (in Finnish). Master's thesis. Helsinki University of Technology, Department of Mechanical Engineering, Ship Laboratory," , 2002, p. 165.

[39] Leisti, H., Kaups, K., Lehtiranta, J., Lindfors, M., Suomminen, M., Lensu, M., Haapala, J., Riska, K. & Kouts, T., "Observation of ships in compressive ice," Montreal, Canada, 2011.

[40] Pärn O., Haapala J., Kõuts T., Elken J. & Riska K., "On the Relationship Between Sea Ice Deformation and Ship Damages in the Gulf of Finland in Winter 2003, Proc. Estonian Acad. Sci. Eng.," , 2007, p. 14.

[41] Jalonen, R. & Ilves, L., "Experience with a Chemically-Doped Fine-Grained Model Ice," in *IAHR Ice Symposium 1990*, vol. 2, Espoo, Finland, August 1990.

[42] Vance, G.P., "A scaling system for vessels modeled in ice," in *SNAME Symposium Ice-Tech '75*, Montreal, 1975.

[43] Kujala, P. & Riska, K., "Talvimerenkulku (TKK-AM-13-2010)," Helsinki University of Technology, Espoo, 2010.

[44] Suominen, M. & Kujala, P., "Ice Model Tests in Compressive Ice," in *21st IAHR International Symposium on Ice*, Dalian, China, June 11 to 15, 2012.

[45] INTERNATIONAL STANDARD ISO 19906, *Petroleum and natural gas industries - Arctic offshore structures*, First edition ed.: Published in Switzerland, 2010-12-15.

APPENDIX

Table 14 *The highest calculated line load for different line load width in each compressive level ice test.*

Test #	$Q_{bowsholder}$ [N/m]	$Q_{midship}$ [N/m]	Q_{PP1} [N/m]	Q_{PP2} [N/m]	Q_{PP3} [N/m]	Q_{PP4} [N/m]
Test1_2	1123,8	456,2	364,4	312,5	274,7	-
Test2_2	584,1	383,6	412,2	210,5	141,2	-
Test3_2	307,6	33,2	182,1	125,0	84,6	-
Test4_2	602,7	576,5	414,1	294,4	235,6	197,5
Test5_2	592,7	141,5	511,6	365,6	251,6	186,4
Test6_2	349,7	121,3	358,8	248,4	170,6	139,5

Table 15 *The highest line loads at bow shoulder, midship and pusher plates in the 1st test series.*

Test #	$Q_{bowsholder}$ [N/m]	$Q_{midship}$ [N/m]	Q_{PP1} [N/m]	Q_{PP2} [N/m]	Q_{PP3} [N/m]	Q_{PP4} [N/m]
Test1_3	2347,4	1976,6	596,1	452,7	372,8	-
Test1_4	1212,9	1852,0	607,3	307,7	205,4	-
Test1_5	1539,2	1088,7	543,5	290,4	201,2	-

Table 16 *The highest line loads at bow shoulder, midship and pusher plates in the 2nd test series.*

Test #	$Q_{bowsholder}$ [N/m]	$Q_{midship}$ [N/m]	Q_{PP1} [N/m]	Q_{PP2} [N/m]	Q_{PP3} [N/m]	Q_{PP4} [N/m]
Test2_3	886,2	879,4	356,9	178,7	120,4	-
Test2_4	839,5	714,4	283,4	170,2	131,4	-
Test2_5	804,3	812,2	233,9	158,4	117,9	-
Test2_6	801,4	824,2	165,8	121,8	86,2	-

Table 17 *The highest line loads at bow shoulder, midship and pusher plates in the 3rd test series.*

Test #	$Q_{bowsholder}$ [N/m]	$Q_{midship}$ [N/m]	Q_{PP1} [N/m]	Q_{PP2} [N/m]	Q_{PP3} [N/m]	Q_{PP4} [N/m]
Test3-3	871,8	385,4	50,1	36,4	26,6	-
Test3_4	-	-	141,0	97,6	81,3	-
Test3_5	352,5	211,2	55,1	50,8	47,9	-
Test3_6	372,9	380,9	108,3	90,0	78,6	-

Table 18 *The highest line loads at bow shoulder, midship and pusher plates in the 4th test series.*

Test #	$Q_{bowsholder}$ [N/m]	$Q_{midship}$ [N/m]	Q_{PP1} [N/m]	Q_{PP2} [N/m]	Q_{PP3} [N/m]	Q_{PP4} [N/m]
Test4_3	562,8	367,0	272,3	179,9	149,2	118,3
Test4_4	767,3	462,6	460,3	267,0	178,1	133,7
Test4_5	892,5	732,9	239,8	201,8	143,7	134,0
Test4_6	805,1	968,6	240,9	195,2	172,7	155,9

Table 19 *The highest line loads at bow shoulder, midship and pusher plates in the 5th test series.*

Test #	$Q_{bowsholder}$ [N/m]	$Q_{midship}$ [N/m]	Q_{PP1} [N/m]	Q_{PP2} [N/m]	Q_{PP3} [N/m]	Q_{PP4} [N/m]
Test5_3	824,0	508,0	301,5	180,8	131,7	111,2
Test5_4	734,0	809,1	412,0	230,0	155,5	135,4
Test5_5	744,6	856,5	183,7	187,6	125,0	131,4
Test5_6	744,6	671,4	288,5	196,4	143,1	117,6
Test5-8	972,0	742,5	387,3	221,6	153,5	115,2
Test5_9	619,5	572,2	224,5	173,3	115,7	86,5

Table 20 *The highest line loads at bow shoulder, midship and pusher plates in the 6th test series.*

Test #	$Q_{bowsholder}$ [N/m]	$Q_{midship}$ [N/m]	Q_{PP1} [N/m]	Q_{PP2} [N/m]	Q_{PP3} [N/m]	Q_{PP4} [N/m]
Test6_3	502,0	275,3	150,9	78,2	61,4	40,7
Test6_4	493,6	485,3	79,5	63,6	46,6	45,5
Test6_5	622,5	529,6	149,1	105,8	90,1	81,5
Test6_6	707,0	542,9	171,7	114,1	102,6	93,4
Test6_8	685,7	731,7	186,0	139,3	117,0	128,2
Test6_9	847,0	833,0	200,0	120,7	124,8	103,5
Test6_10	648,8	618,8	180,4	106,0	110,2	95,6